Available online at www.sciencedirect.com
ScienceDirect
Chemie der Erde 68 (2008) 155–176
CHEMIE der ERDE GEOCHEMISTRY
www.elsevier.de/chemer

The relationship between collision-related calcalkaline, and within-plate alkaline volcanism in the Karacadağ Area (Konya-Türkiye, Central Anatolia)

Hüseyin Kurt[a,*], Kürşad Asan[a], Gilles Ruffet[b]

[a]*Department of Geological Engineering, Selçuk University, Konya, 42079, Türkiye*
[b]*Geosciences Rennes, CNRS-Université de Rennes 1, Campus de Beaulieu, Avenue Général Leclerc, Rennes Cedex, 35042, France*

Received 6 June 2005; accepted 25 April 2006

Abstract

The Karacadağ (Kulu-Konya) area is one of the main volcanic provinces in Central Anatolia. The Karacadağ volcanites are composed of large volumes of andesitic-dacitic lavas associated with pyroclastics and small volumes of alkali basalt, trachybasalt and trachyandesite lavas. Two groups of volcanic rocks can be distinguished: (1) calcalkaline rocks including andesites and dacites, and (2) alkaline rocks including basalts, trachybasalts and trachyandesites. $^{40}Ar/^{39}Ar$ ages show that the Karacadağ volcanites were erupted during Early Miocene (ca.18–19 Ma) and suggest that alkaline volcanites succeed shortly afterwards calcalkaline volcanites. Major oxides and trace elements plotted versus SiO_2 suggest fractionation of hornblende, Fe–Ti oxide and apatite for calcalkaline volcanic rocks and olivine, clinopyroxene and Fe–Ti oxide for alkaline volcanic rocks in the magmatic evolution. The incompatible trace element patterns of the calcalkaline volcanites show enrichment of LILEs (Sr, K, Rb, Ba and Th) and negative HFSEs (Nb, Ta) anomalies suggesting an enriched lithospheric source by a subduction-related process. On the other hand, alkaline volcanites show enrichment of both LILEs and HFSEs suggesting an enriched lithospheric source by small volume melts from the asthenosphere. The rocks also have moderately fractionated REE patterns with $(La/Lu)_N$ ratios of 7–24 for calcalkaline and 6–17 for alkaline volcanites. Moreover, the volcanites have relatively low $^{87}Sr/^{86}Sr(t)$ ratios for $t = 18$ Ma between 0.703782 and 0.705129, and high $\varepsilon_{Nd}(t)$ values between +2.25 and +4.49. Generally, the Sr–Nd isotopic compositions of the rocks range from the mantle array to bulk earth. All of these observations and findings suggest that the calcalkaline volcanites were formed in a subduction modified orogenic setting, and the alkaline volcanites in a within-plate setting.

Keywords: Central anatolia; Karacadağ volcanites; Alkaline; $^{40}Ar/^{39}Ar$ dating; Within-plate

1. Introduction

Subduction-related and intraplate-type magmatic rocks occur together in many collision zones. Formation of magmas with a subduction-related geochemical signature can result from: (1) subduction of oceanic lithosphere (Hawkesworth et al., 1993; Pearce and Peate, 1995), (2) melting of metasomatically enriched subcontinental lithosphere with inherited subduction signature (Turner et al., 1996; Benito et al., 1999), or (3) extensive crustal contamination of MORB-like magmas (Turner et al., 1999). Generating of intraplate-type lavas in continental settings is generally related to upwelling sub-lithospheric

*Corresponding author. Tel.: +90 332 2232194; fax: 90 332 2410520.
E-mail address: hkurt@selcuk.edu.tr (H. Kurt).

0009-2819/$ - see front matter © 2006 Elsevier GmbH. All rights reserved.
doi:10.1016/j.chemer.2006.05.003

mantle material (Wilson and Downes, 1991; Granet et al., 1995; Hoernle et al., 1995). However, the process responsible for uplift and the generation of volcanic areas with geochemically diverse rock types such as subduction-related and intraplate-type magmatic rocks are still poorly understood (Duggen et al., 2005).

This paper presents geochronological ($^{40}Ar/^{39}Ar$ dating) and geochemical (major elements, trace elements and Sr–Nd isotopes) data in order to study the transition from collision-related to within plate-type volcanism in Central Anatolia.

The study area (Fig. 1) is located approximately 150 km to the north of Konya (Central Anatolia), on the northern margin of the Menderes-Tauride platform, immediately southwest of the Kırşehir block (Central Türkiye). The geology of Türkiye was mainly shaped by the opening and closing of both the Paleo and Neo Tethys oceans and their related marginal basins (Şengör and Yılmaz, 1981; Şengör, 1985; Okay, 1986; Okay et al., 1996; Stampfli et al., 1991, 2001; Stampfli and Borel, 2002; Eren et al., 2004). The neotectonic period started in Türkiye as a result of the collision of the African and Arabian plates along the Helenic arc to the west, and the Bitlis-Zagros zone to the east. This collision led to crustal shortening in Eastern Anatolia and the formation of the North Anatolian Fault (NAF) and the East Anatolian Fault (EAF). The Anatolian block started to move westwards along these main faults (McKenzie, 1972; Şengör et al., 1985; Dewey et al., 1986). Within this compressional strain field, widespread volcanic activity occurred in Eastern, Central and Western Anatolia (Fig. 1).

In Central Anatolia, young volcanic provinces, such as Galatia Volcanites (GV), Central Anatolian Volcanites (CAV) and Konya volcanites (KV), cover large areas. The Galatia Volcanites located within the Pontide tectonic belt of NW Central Anatolia comprise a number of Miocene volcanic complexes. While earlier studies suggested that the Early Miocene volcanism of GV was related to plate convergence including closure of the northern branch of the Neo Tethys ocean through northward subduction (Tankut et al., 1991; Keller et al., 1992), new studies indicate that the parental magmas were generated in a post-collisional tectonic setting from a previously subduction-modified mantle source (Wilson et al., 1997; Tankut et al., 1998). The Central Anatolian Volcanites comprise ignimbrites and two stratovolcanoes (Karacadağ in Karaman and Melendiz) of Mio-Pliocene age, plus a number of monogenetic vents (basaltic maars, cinder cones, felsic maars and domes) and two stratovolcanoes (Erciyes and Hasan) (Aydar et al., 1995) of Quaternary age (Aydar and Gourgaud, 1998). Volcanism in this area is related to continental collision between the Afro-Arabian and Eurasian plates (Pasquare et al., 1988). Upper Miocene-Pliocene Konya volcanites located on SW edge of CAV were regarded as products of subduction of the African plate under the Anatolian block (Innocenti et al., 1975; Temel et al., 1998; Kurt et al., 2003). However, a few studies have been done on the origin of Karacadağ volcanites around Konya. Asan (2002) firstly showed that volcanism in this area was related to a subduction event, and calkalkaline and alkaline volcanite coexisted.

2. Geological setting

In the study area, basement is an ophiolitic melange. The ophiolitic rocks viewed as part of an accretionary

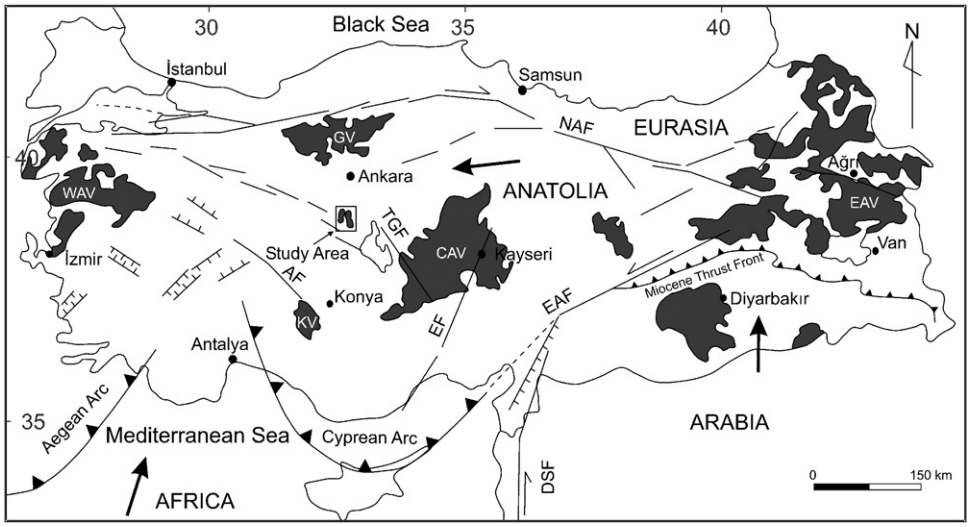

Fig. 1. Location map of Karacadağ volcanites and distribution of Neogene-Quaternary volcanic rocks of Türkiye. (WAV: West Anatolian Volcanites, GV: Galatia volcanites, KV: Konya Volcanites (Erenlerdağ-Alacadağ volcanites), CAV: Central Anatolian Volcanites, EAV: East Anatolian Volcanites, DSF: Dead Sea Fault, NAF: North Anatolian Fault, EAF: East Anatolian Fault, AF: Akşehir Fault, TGF: Tuzgölü Fault, EF: Ecemiş Fault). Map is modified from Ketin (1983) and Koçyiğit (1991).

prism were emplaced during middle to late Maastrichtian (Göncüoğlu et al., 1991, 1996), in relation with the closure of the northern branch of Neo Tethys. This basement is unconformably overlain by Late Cretaceous to Eocene sediments including the Maastrichtian Haymana formation, the Paleocene Çaldağ and Kırkavak formations, the Eocene Eskipolatlı formation (Görür et al., 1984). The Mio-Pliocene Cihanbeyli formation, interfingered with the Miocene Karacadağ volcanites, unconformably overlies all these units (Fig. 2).

3. Method and analytical techniques

3.1. Geochronology $^{40}Ar/^{39}Ar$

Analyses were performed on single whole-rock fragments with an ^{39}Ar–^{40}Ar laser probe (CO_2 Synrad®) and a Map215® mass spectrometer. Whole-rock fragments were carefully handpicked under a binocular microscope from crushed rocks (0.3–2 mm fraction). The samples were wrapped in A1 foil to form packets (11 mm × 11 mm × 0.5 mm). These packets were stacked up to form a pile, within which packets of flux monitors were inserted every 8–10 samples. The stack, put in an irradiation can, was irradiated for 40 h at the McMaster reactor (Hamilton, Canada) with a total flux of 5×10^{18} n cm^{-2}. The irradiation standard was the sanidine TCR-2 (28.34 Ma according to Renne et al., 1998). The sample arrangement allowed us to monitor the flux gradient with a precision of ±0.2%. The step-heating experimental procedure has been described in detail by Ruffet et al. (1995, 1997). Blanks are performed routinely each first or third run, and are subtracted from the subsequent sample gas fractions.

To define a plateau age, a minimum of three consecutive steps are required, corresponding to a minimum of 70% of the total $^{39}Ar_K$ released, and the individual fraction ages should agree to within 1σ or 2σ with the integrated age of the plateau segment. All discussed ^{39}Ar–^{40}Ar results are displayed at the 1σ level. The errors do not include the error in the value of the J parameter (Table 1).

3.2. Microprobe analyses

Mineral analyses were performed using a JEOL 8900 Electron Probe Microanalyzer at the McGill University Microprobe Laboratory (Canada). Operating conditions were: 15 kV accelerating voltage (20 kV for olivine), 20 nA beam current and 20 s counting time per each element (60 s for Ni). However, it should be noted that the Fe–Ti oxide analyses suffer from low totals. So, the Fe–Ti oxide analyses results were not shown on the tables.

3.3. Chemical analyses

Major and trace elements were analyzed by ICP-ES and rare earth elements were analyzed by ICP/MS at ACME Laboratories (Canada).

3.4. Isotopic analyses

Sr–Nd isotope compositions for 12 whole rock samples were determined using a Finnigan Mat 262 mass spectrometer and performed at Geosciences Rennes, France (Table 2). Total blanks were: Rb = 0.1 ng, Sr–Nd–Sm < 0.05 ng. Uncertainties are 2% for $^{87}Rb/^{86}Sr$ ratios and 0.2% for $^{147}Sm/^{144}Nd$ ratios. Replicate analyses of NBS 987 yield a mean $^{87}Sr/^{86}Sr$ ratio of 0.71020 ± 8 and a mean $^{143}Nd/^{144}Nd$ ratio of 0.511962 ± 6 for AMES standard.

4. Geochronology $^{40}Ar/^{39}Ar$ of some Karacadağ volcanites

According to field observations, geochronologic and petrologic studies, the Karacadağ volcanites can be seperated into two magmatic suites with calcalkaline and alkaline characters, respectively. In the study area, the volcanic sequence begins with large pyroclastic deposits and continues with porphyritic andesitic and dacitic domes and lava flows, which are calcalkaline in character. Samples from a dacitic dome (KU45) and from an andesitic lava flow (KU104) yielded plateau ages of 19.2 ± 0.1 and 19.0 ± 0.1 Ma, respectively (Fig. 3). This calcalkaline volcanic activity was followed by small lava flows and dykes of alkaline volcanites including aphanitic to olivine phyric basalt-trachybasalt, scoria and plagioclase phyric trachyandesite. $^{40}Ar/^{39}Ar$ dating of one alkali basalt (KU153) and one trachyandesite (KU174) yielded $^{40}Ar/^{39}Ar$ plateau age of 18.8 ± 0.2 and 18.1 ± 0.1 Ma, respectively (Fig. 3). So, the $^{40}Ar/^{39}Ar$ ages are consistent with field observation pointing that volcanic activity took place during the Lower Miocene. These results also suggest that the transition from calcalkaline to alkaline volcanism occurred over a short time-span.

5. Petrography and chemical composition of minerals

5.1. Calcalkaline volcanites

The calcalkaline volcanites of the Karacadağ area are designated as hornblende andesite, pyroxene andesite, dacite porphyry and dacite based on their mineralogical, petrographic and textural characteristics (Tables 3–5).

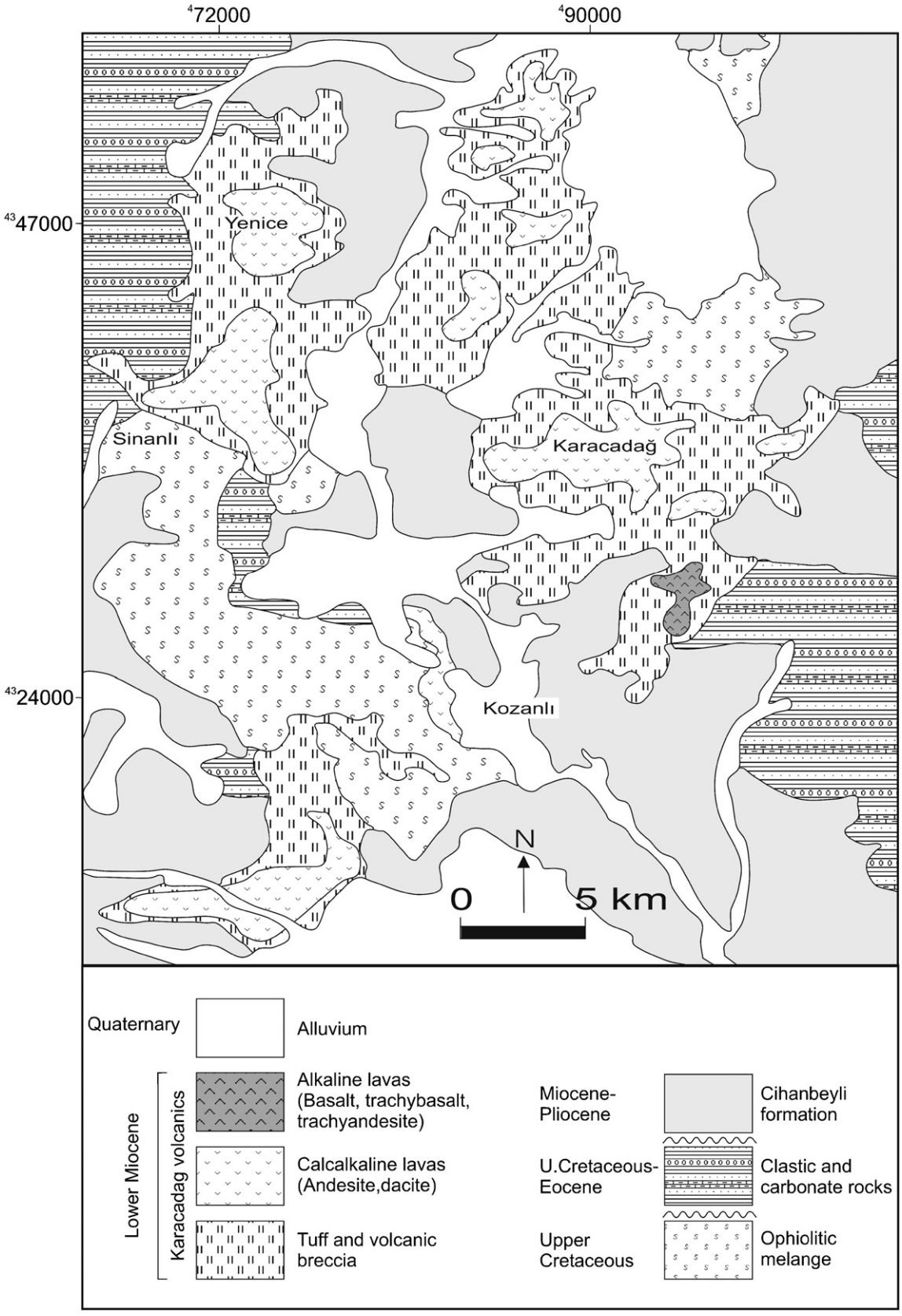

Fig. 2. Geological sketch map of the studied area (modified from Şenel, 2001).

Table 1. $^{40}Ar/^{39}Ar$ analytical data

Step	$^{40}Ar_{Atm.}$ (%)	$^{39}Ar_K$ (%)	$^{37}Ar_{Ca}/^{39}Ar_K$	$^{40}Ar^*/^{39}Ar_K$	Age (Ma)
KU45 Dacite Whole Rock			$J = 0.00880094$		
1	85.0	1.3	0.3350	1.10	17.5±2.6
2	11.4	2.6	0.2740	1.20	18.9±1.1
3	1.3	11.5	0.3180	1.29	20.4±0.2
4	1.4	14.4	0.3850	1.23	19.5±0.2
5	0.2	15.9	0.4240	1.21	19.1±0.2
6	0.0	16.5	0.4400	1.21	19.1±0.4
7	0.0	14.1	0.5230	1.23	19.4±0.3
8	1.3	9.4	0.6710	1.19	18.7±0.4
9	0.0	8.3	0.9590	1.21	19.2±0.3
Fusion	1.9	6.1	3.9030	1.21	19.1±0.6
				Integrated age:	19.3±0.1
KU104 Andesite Whole Rock			$J = 0.00879605$		
1	98.1	2.1	0.0000	0.37	5.9±5.1
2	81.7	3.4	0.0000	0.39	6.2±1.2
3	23.1	4.0	0.6150	0.76	12.0±0.9
4	7.3	11.2	0.4020	1.19	18.8±0.3
5	3.2	10.6	0.0580	1.27	20.0±0.4
6	2.4	9.7	0.0050	1.26	19.9±0.4
7	2.9	22.2	0.3650	1.21	19.2±0.2
8	3.9	13.9	0.4410	1.16	18.4±0.4
9	2.8	10.0	1.1100	1.17	18.4±0.4
10	3.3	6.4	1.2590	1.17	18.4±0.5
11	21.6	3.1	1.4610	0.96	15.2±0.9
Fusion	35.3	3.4	3.3090	0.91	14.4±0.9
				Integrated age:	17.8±0.2
KU153 Alkali Basalt Whole Rock			$J = 0.00877655$		
1	95.2	0.1	1.6030	0.15	2.4±26.9
2	85.3	0.3	1.4400	0.83	13.1±14.2
3	34.0	0.3	1.4300	1.68	26.3±11.7
4	17.6	0.9	1.5140	1.39	21.8±3.1
5	23.3	2.5	1.5600	1.21	19.1±1.5
6	12.9	2.8	0.9060	1.19	18.7±0.9
7	10.2	5.0	0.7750	1.18	18.5±0.8
8	0.1	4.4	0.7400	1.24	19.6±0.9
9	2.0	7.6	0.9690	1.21	19.1±0.4
10	0.0	4.7	1.2210	1.26	19.8±0.7
11	0.0	5.1	1.4590	1.27	20.0±0.9
12	6.4	4.6	1.6700	1.15	18.1±0.8
13	2.3	6.9	1.5810	1.19	18.7±0.5
14	2.3	5.2	1.9470	1.19	18.7±0.9
Fusion	1.5	49.5	2.9130	1.18	18.6±0.3
				Integrated age:	18.8±0.2
KU174 Tracyandesite Whole Rock			$J = 0.00877169$		
1	30.5	6.4	0.2320	1.14	18.0±0.5
2	4.2	8.3	0.2370	1.17	18.5±0.3
3	0.6	8.8	0.2690	1.18	18.6±0.2
4	1.6	11.5	0.3140	1.15	18.1±0.2
5	0.2	11.6	0.4030	1.15	18.1±0.3
6	0.0	11.0	0.5880	1.14	17.9±0.3
7	0.0	9.9	0.8330	1.13	17.8±0.3
8	1.9	10.2	1.1930	1.10	17.3±0.3
9	0.9	7.7	1.2680	1.09	17.2±0.3
10	1.2	5.6	1.4200	1.06	16.6±0.4
11	3.4	3.5	1.7310	1.03	16.2±0.6

Table 1. (*continued*)

Step	$^{40}Ar_{Atm.}$ (%)	$^{39}Ar_K$ (%)	$^{37}Ar_{Ca}/^{39}Ar_K$	$^{40}Ar^*/^{39}Ar_K$	Age (Ma)
12	13.9	1.7	1.7070	0.92	14.5 ± 1.3
Fusion	1.3	3.9	1.2350	1.09	177.2 ± 0.6
				Integrated age:	17.0 ± 0.1

$^{40}Ar_{atm}$ = atmospheric ^{40}Ar; $^{40}Ar^*$ = radiogenic ^{40}Ar; Ca = produced by Ca-neutron interferences; K = produced by K-neutron interferences. Age (Ma) = the date is calculated using the decay constants recommended by Steiger and Jäger (1977). Correction factors for interfering isotopes produced by neutron irradiation in the McMaster reactor were $(^{39}Ar/^{37}Ar)_{Ca} = 7.06 \times 10^{-4}$; $(^{36}Ar/^{37}Ar)_{Ca} = 2.79 \times 10^{-4}$; $(^{40}Ar/^{39}Ar)_K = 2.95 \times 10^{-2}$.

Table 2. Sr and Nd isotopic analyses of the Karacadağ volcanites

Sample	Rock type	$^{87}Sr/^{86}Sr$	±2σm	$^{87}Sr/^{86}Sr$ corrected ratios $t = 18$ Ma	$^{143}Nd/^{144}Nd$	±2σm	ε corrected $t = 18$ Ma
KA-154	Alkali basalt	0.703802	0.000007	0.703782	0.5128620	0.000004	4.49
KA-13	Alkali basalt	0.704651	0.000006	0.704616	0.5128190	0.000004	3.68
KA-8	Trachybasalt	0.705165	0.000007	0.705129	0.5127590	0.000005	2.52
KA-104	Hornblende andesite	0.704493	0.000008	0.704448	0.5128040	0.000005	3.41
KA-25	Hornblende andesite	0.704872	0.000010	0.704811	0.5127470	0.000004	2.31
KA-24	Hornblende andesite	0.704840	0.000006	0.704874	0.5127440	0.000004	2.25
KA-90	Hornblende andesite	0.704501	0.000008	0.704448	0.5128250	0.000004	3.81
KA-49	Trachyandesite	0.704732	0.000007	0.704649	0.5127800	0.000004	2.94
KA-307-2	Trachyandesite	0.704611	0.000008	0.704535	0.5128010	0.000004	3.34
KA-296-2	Trachyandesite	0.704782	0.000008	0.704695	0.5127540	0.000004	2.46
KA-299-2	Trachyandesite	0.704865	0.000007	0.704824	0.5127780	0.000004	2.89
KA-45	Dacite porphyry	0.704936	0.000009	0.704889	0.5128220	0.000005	3.75

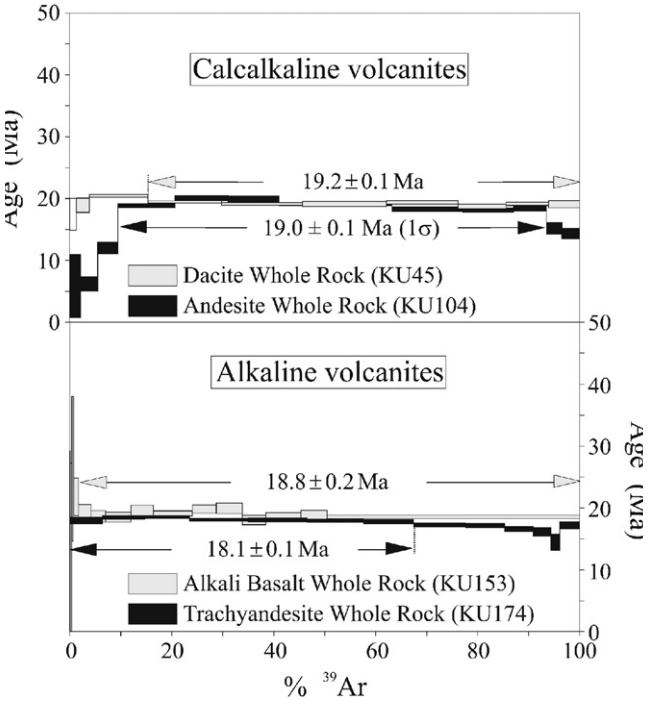

Fig. 3. ^{39}Ar–^{40}Ar age spectra of four whole rock fragments of volcanic rocks from Karacadağ area. The age error bars for each temperature steps are at the 1σ level and do not include errors in the *J*-values. The errors in the *J*-values are included in the plateau age calculations.

Hornblende andesites have hypocrystalline porphyritic texture with phenocrysts of plagioclase, hornblende, ortho and clinopyroxene and subordinate titanomagnetite. The groundmass has a hyalopilitic texture, and includes plagioclase microlites and volcanic glass. Plagioclase is andesine to labradorite (An_{32-53}) (Fig. 4), with reverse and oscillatory zoning. In addition, sieve texture, overgrowth and resorption are observed in plagioclase. Amphibole is pargasite, following the nomenclature of Leake et al. (1997) (Fig. 5). Hornblende has opaque rims, but an important compositional change from core to rim has not been recorded. Clinopyroxene is augite and orthopyroxene enstatite in composition, according to the classification of Morimoto et al. (1988) (Fig. 6). While the composition of the augite core sections are $Wo_{44}En_{45-46}Fs_{10-11}$ with $Mg\# = Mg/(Mg + Fe^{tot})$ 0.83, the composition of its rim are $Wo_{42-43}En_{44-45}Fs_{13-14}$ with $Mg\# = 0.76$, conforming to normal zoning. The composition of enstatite is $Wo_3En_{75}Fs_{22}$. Fe–Ti oxides are magnetite (Fig. 7).

Pyroxene andesites exhibit hypocrystalline porphyritic texture with phenocrysts of plagioclase, ortho and clinopyroxene and subordinate Fe–Ti oxide (ulvöspinel). The groundmass has a hyalopilitic texture and includes plagioclase microlites, ortho- and clinopyroxene,

Table 3. Selected microprobe analyses of amphibole from the Karacadağ volcanites

	Hornblende andesite							Dacite						Dacite porphyr			
(wt%)	Hb-1a	Hb-1b	Hb-1c	Hb-2	Hb-5	Hb-6a	Hb-6b	Hb-7a	Hb-7b	Hb-10a	Hb-10b	Hb-13	Hb-14	Hb-16a	Hb-16b	Hb-17	Hb-18
SiO_2	41.87	41.33	41.18	41.12	42.80	41.60	41.04	46.61	48.22	48.06	48.14	46.90	46.35	43.77	42.60	41.09	41.03
TiO_2	4.02	3.93	3.45	4.22	2.51	4.06	4.18	1.70	1.38	1.13	1.26	1.15	1.20	2.40	2.33	3.76	3.43
Al_2O_3	11.90	12.04	11.65	12.14	11.08	11.58	12.11	7.98	6.81	7.34	6.84	8.97	9.00	11.60	11.68	13.34	13.06
FeO	12.10	12.29	13.12	11.17	12.97	11.38	11.32	12.66	11.87	12.99	11.97	10.85	11.39	11.36	12.19	10.18	10.69
MnO	0.15	0.22	0.20	0.12	0.20	0.11	0.17	0.26	0.25	0.38	0.31	0.17	0.18	0.20	0.23	0.13	0.12
MgO	13.77	13.72	13.00	13.88	13.82	14.42	14.05	14.95	16.00	15.28	16.20	15.81	15.33	15.00	14.14	14.73	14.37
CaO	11.03	10.94	10.72	11.01	10.97	11.04	11.06	11.08	11.20	10.57	10.73	11.22	11.03	11.10	10.89	11.03	11.00
Na_2O	2.74	2.75	2.64	2.70	2.46	2.71	2.69	1.65	1.39	1.43	1.39	1.68	1.65	3.30	3.09	3.00	3.03
K_2O	0.56	0.60	0.57	0.59	0.50	0.62	0.62	0.29	0.21	0.27	0.24	0.16	0.19	0.33	0.33	0.59	0.61
Cr_2O_3	0.01	0.05	0.00	0.04	0.00	0.04	0.04	0.00	0.03	0.05	0.00	0.15	0.30	0.02	0.03	0.03	0.01
Total	98.15	97.88	96.54	96.99	97.30	97.56	97.28	97.15	97.36	97.49	97.09	97.08	96.61	99.07	97.51	97.87	97.34
Formula on the basis of 23 oxygens																	
Si	6.16	6.11	6.19	6.10	6.35	6.14	6.08	6.84	7.00	7.01	7.01	6.81	6.79	6.33	6.29	6.01	6.05
Al ^{IV}	1.84	1.89	1.81	1.90	1.65	1.86	1.92	1.16	1.00	0.99	0.99	1.19	1.21	1.67	1.71	1.99	1.95
Al ^{VI}	0.22	0.21	0.25	0.22	0.29	0.16	0.20	0.22	0.17	0.27	0.18	0.35	0.34	0.31	0.32	0.32	0.32
Al ^{tot}	2.06	2.10	2.06	2.12	1.94	2.02	2.12	1.38	1.17	1.26	1.17	1.54	1.55	1.98	2.03	2.31	2.27
Ti	0.44	0.44	0.39	0.47	0.28	0.45	0.47	0.19	0.15	0.12	0.14	0.13	0.13	0.26	0.26	0.41	0.38
Cr	0.00	0.01	0.00	0.00	0.00	0.00	0.00	0.00	0.00	0.01	0.00	0.02	0.03	0.00	0.00	0.00	0.00
Fe^{2+}	1.49	1.52	1.65	1.39	1.61	1.40	1.40	1.50	1.35	1.57	1.36	1.25	1.32	1.37	1.51	1.25	1.32
Fe^{3+}	0.00	0.00	0.00	0.00	0.00	0.00	0.00	0.05	0.10	0.02	0.10	0.07	0.07	0.00	0.00	0.00	0.00
Mn	0.02	0.03	0.03	0.01	0.03	0.01	0.02	0.03	0.03	0.05	0.04	0.02	0.02	0.02	0.03	0.02	0.01
Mg	3.02	3.02	2.91	3.07	3.06	3.17	3.10	3.27	3.46	3.32	3.51	3.42	3.35	3.23	3.11	3.21	3.16
FMT	13.19	13.23	13.23	13.16	13.27	13.19	13.19	13.26	13.26	13.36	13.33	13.26	13.26	13.19	13.23	13.21	13.19
Ca	1.74	1.73	1.73	1.75	1.74	1.75	1.76	1.74	1.74	1.65	1.67	1.75	1.73	1.72	1.72	1.73	1.74
Na (B)	0.07	0.05	0.05	0.08	0.00	0.05	0.05	0.00	0.00	0.00	0.00	0.00	0.00	0.08	0.04	0.06	0.06
Na (A)	0.71	0.74	0.72	0.70	0.71	0.73	0.72	0.47	0.39	0.40	0.39	0.47	0.47	0.85	0.84	0.79	0.81
Na ^{tot}	0.78	0.79	0.77	0.78	0.71	0.78	0.77	0.47	0.39	0.40	0.39	0.47	0.47	0.93	0.88	0.85	0.87
K	0.10	0.11	0.11	0.11	0.09	0.12	0.12	0.05	0.04	0.05	0.04	0.03	0.04	0.06	0.06	0.11	0.11
Sum A	0.81	0.85	0.83	0.81	0.80	0.85	0.84	0.52	0.43	0.45	0.43	0.50	0.51	0.91	0.90	0.90	0.92
Mg#	0.67	0.67	0.64	0.69	0.66	0.69	0.69	0.68	0.70	0.68	0.71	0.72	0.71	0.70	0.67	0.72	0.71

Fe^{2+} and Fe^{3+} estimated according to Droop (1987).

Table 4. Selected microprobe analyses of pyroxene from the Karacadağ volcanites

	Hornblende andesite			Pyroxene andesite			Dacite			Trachyandesite				Alkali basalt			
(wt%)	px-10	px-11	px-13c	px-28	px-29	px-30a	px-14	px-15	px-16	px38a	px38b	px39a	px39b	px-1a	px-1b	px-2a	px-2b
SiO_2	49.78	50.32	53.94	52.54	52.47	53.57	53.26	53.43	52.42	52.78	53.85	52.28	52.69	50.36	47.99	49.99	48.03
TiO_2	1.02	0.92	0.23	0.24	0.48	0.14	0.09	0.13	0.1	0.35	0.15	0.47	0.39	1.1	1.71	1.38	1.66
Al_2O_3	4.38	3.88	1.3	1.23	2.07	0.57	0.71	0.73	0.39	3.21	1.35	2.44	1.53	4.04	6.33	4.33	6.6
FeO	8.59	8.46	13.9	8.2	5.9	20.15	20.44	20.54	19.9	14.01	15.52	7.01	8.31	6.03	6.37	6.71	6.12
MnO	0.22	0.2	0.34	0.3	0.18	0.66	0.88	0.84	0.83	0.29	0.34	0.2	0.24	0.12	0.12	0.14	0.14
MgO	15.34	15.08	27.67	15.11	17.78	24.15	23.68	23.49	23.56	27.05	26.88	16.33	16.1	15.44	14.19	15.14	14.24
CaO	19.64	20.24	1.4	21.79	20.21	0.91	0.66	0.89	1.9	1.6	1.12	20.69	20.37	21.95	22.14	21.89	22.04
Na_2O	0.49	0.54	0.06	0.33	0.24	0	0	0.02	0	0.03	0	0.35	0.27	0.41	0.48	0.39	0.46
K_2O	0.01	0.02	0.01	0.03	0.01	0.01	0.01	0.02	0.01	0.02	0.01	0.02	0.01	0.01	0.01	0	0.02
Cr_2O_3	0.03	0.01	0	0	0.12	0	0	0.01	0	0.01	0.13	0.02	0.01	0.29	0.47	0.12	0.62
NiO	0	0	0	0	0	0	0	0	0	0	0	0	0	0	0	0	0.01
Total	99.5	99.66	98.86	99.76	99.47	100.15	99.72	100.09	99.12	99.36	99.36	99.82	99.91	99.76	99.8	100.09	99.93
Formula on the basis of 6 oxygens																	
Si	1.86	1.88	1.96	1.96	1.93	1.97	1.98	1.98	1.96	1.91	1.96	1.93	1.95	1.87	1.79	1.85	1.78
Ti	0.03	0.03	0.01	0.01	0.01	0	0	0	0	0.01	0	0.01	0.01	0.03	0.05	0.04	0.05
Al	0.19	0.17	0.06	0.05	0.09	0.02	0.03	0.03	0.02	0.14	0.06	0.11	0.07	0.18	0.28	0.19	0.29
Fe^{2+}	0.17	0.17	0.39	0.2	0.13	0.59	0.61	0.62	0.54	0.38	0.45	0.17	0.22	0.11	0.09	0.13	0.09
Fe^{3+}	0.10	0.09	0.03	0.06	0.05	0.03	0.02	0.02	0.08	0.04	0.02	0.05	0.04	0.08	0.11	0.08	0.1
Mn	0.01	0.01	0.01	0.01	0.01	0.02	0.03	0.03	0.03	0.01	0.01	0.01	0.01	0	0	0	0
Mg	0.85	0.84	1.5	0.84	0.98	1.33	1.31	1.29	1.32	1.46	1.46	0.9	0.89	0.85	0.79	0.84	0.79
Ca	0.79	0.81	0.05	0.87	0.8	0.04	0.03	0.04	0.08	0.06	0.04	0.82	0.81	0.87	0.88	0.87	0.88
Na	0.04	0.04	0	0.02	0.02	0	0	0	0	0	0	0.03	0.02	0.03	0.03	0.03	0.03
K	0	0	0	0	0	0	0	0	0	0	0	0	0	0	0	0	0
Cr	0	0	0	0	0	0	0	0	0	0	0	0	0	0.01	0.01	0	0.02
Ni	0	0	0	0	0	0	0	0	0	0	0	0	0	0	0	0	0
Total	4.03	4.03	4.01	4.02	4.02	4.01	4.01	4.01	4.03	4.01	4.01	4.02	4.01	4.03	4.04	4.03	4.03
Mg#	0.76	0.76	0.78	0.77	0.84	0.68	0.67	0.67	0.68	0.78	0.76	0.81	0.78	0.82	0.8	0.8	0.81
Wo	41.04	42.19	2.75	44.07	40.67	1.79	1.31	1.77	3.74	3.18	2.2	42.19	41.2	45.56	47.16	45.32	47.16
En	44.6	43.73	75.48	42.52	49.78	66.19	65.56	65.01	64.44	74.68	73.47	46.33	45.31	44.59	42.06	43.61	42.4
Fs	14.37	14.08	21.78	13.42	9.55	32.01	33.13	33.22	31.83	22.15	24.33	11.48	13.5	9.85	10.78	11.07	10.45

Fe^{2+} and Fe^{3+} estimated according to Droop (1987).

Table 5. Selected microprobe analyses of olivine from the Karacadağ volcanites

(wt%)	Alkali basalt Ol-1a	Ol-1b	Ol-2a	Ol-2b	Ol-2	Ol-3a	Ol-3b	Ol-4a	Ol-4b	Ol-5a	Ol-5b	Ol-6a
SiO_2	39.67	38.33	39.32	39.65	39.23	40.79	39.77	39.81	38.90	38.98	39.64	40.51
TiO_2	0.00	0.03	0.01	0.00	0.01	0.00	0.00	0.00	0.00	0.01	0.00	0.02
Al_2O_3	0.06	0.16	0.03	0.03	0.02	0.05	0.05	0.02	0.03	0.04	0.03	0.06
FeO	13.30	20.51	17.54	15.86	17.46	10.77	15.52	17.25	21.77	20.12	16.62	10.75
MnO	0.21	0.49	0.30	0.28	0.30	0.16	0.29	0.28	0.42	0.39	0.29	0.15
MgO	46.43	39.92	42.79	44.30	42.39	48.37	44.44	43.15	39.31	40.60	43.28	48.41
CaO	0.22	0.28	0.25	0.22	0.27	0.22	0.19	0.26	0.28	0.26	0.24	0.25
Na_2O	0.00	0.01	0.01	0.01	0.00	0.01	0.01	0.01	0.00	0.00	0.01	0.00
K_2O	0.01	0.03	0.02	0.03	0.01	0.02	0.02	0.02	0.02	0.01	0.01	0.01
Cr_2O_3	0.01	0.06	0.02	0.02	0.02	0.03	0.02	0.00	0.00	0.02	0.05	0.05
NiO	0.12	0.06	0.07	0.10	0.07	0.24	0.13	0.08	0.04	0.05	0.08	0.24
Total	100.04	99.89	100.35	100.49	99.78	100.66	100.44	100.88	100.77	100.46	100.26	100.45
Formula on the basis of 4 oxygens												
Si	0.99	0.99	1.00	1.00	1.00	1.00	1.00	1.00	1.00	1.00	1.00	0.99
Ti	0.00	0.00	0.00	0.00	0.00	0.00	0.00	0.00	0.00	0.00	0.00	0.00
Al	0.00	0.01	0.00	0.00	0.00	0.00	0.00	0.00	0.00	0.00	0.00	0.00
Fe	0.28	0.44	0.37	0.33	0.37	0.22	0.33	0.36	0.47	0.43	0.35	0.22
Mn	0.00	0.01	0.01	0.01	0.01	0.00	0.01	0.01	0.01	0.01	0.01	0.00
Mg	1.73	1.54	1.62	1.66	1.61	1.77	1.66	1.62	1.51	1.55	1.63	1.77
Ca	0.01	0.01	0.01	0.01	0.01	0.01	0.01	0.01	0.01	0.01	0.01	0.01
Na	0.00	0.00	0.00	0.00	0.00	0.00	0.00	0.00	0.00	0.00	0.00	0.00
K	0.00	0.00	0.00	0.00	0.00	0.00	0.00	0.00	0.00	0.00	0.00	0.00
Cr	0.00	0.00	0.00	0.00	0.00	0.00	0.00	0.00	0.00	0.00	0.00	0.00
Ni	0.00	0.00	0.00	0.00	0.00	0.00	0.00	0.00	0.00	0.00	0.00	0.00
Total	3.01	3.00	3.00	3.00	3.00	3.00	3.00	3.00	3.00	3.00	3.00	3.00
Mg#	0.86	0.78	0.81	0.83	0.81	0.89	0.84	0.82	0.76	0.78	0.82	0.89
Fo	85.96	77.20	81.04	83.03	80.97	88.75	83.36	81.43	75.93	77.91	82.02	88.78
Fa	13.82	22.26	18.64	16.67	18.71	11.09	16.33	18.27	23.60	21.66	17.67	11.07

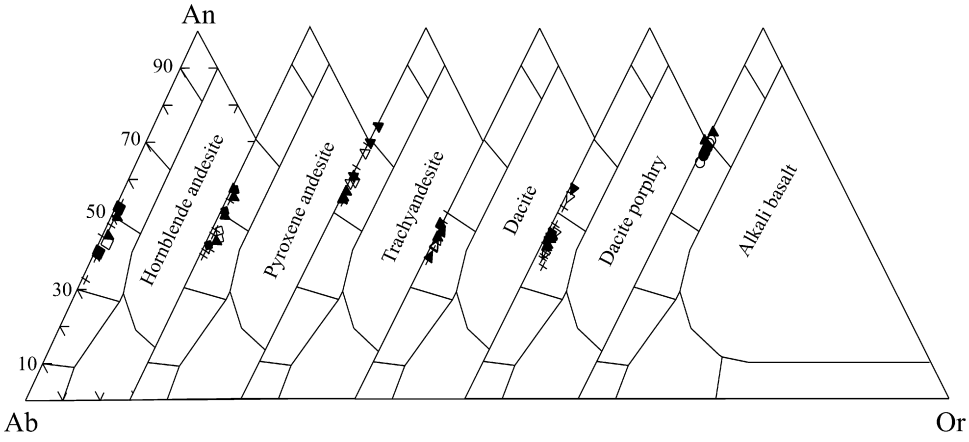

Fig. 4. Ternary An–Ab–Or plot of plagioclases (solid symbol: core, open symbol: rim, plus sign: middle).

Fe–Ti oxide and volcanic glass. Plagioclase is andesine to labradorite in composition (An_{38-56}) (Fig. 4), with oscillatory zoning. Sieve textures are widespread in plagioclase. The composition of the clinopyroxene (augite) is $Wo_{41-43}En_{50-43}Fs_{9-13}$ with Mg# of 0.77 – 0.85. Orthopyroxene (enstatite) shows a small compositional difference between core ($Wo_2En_{65-67}Fs_{32-33,}$ Mg# = 0.67) and rim ($Wo_2En_{67}Fs_{31-32,}$ Mg# = 0.69), conforming to reverse zoning (Fig. 6). Some orthopyroxene phenocrysts were mantled by clinopyroxene. Such

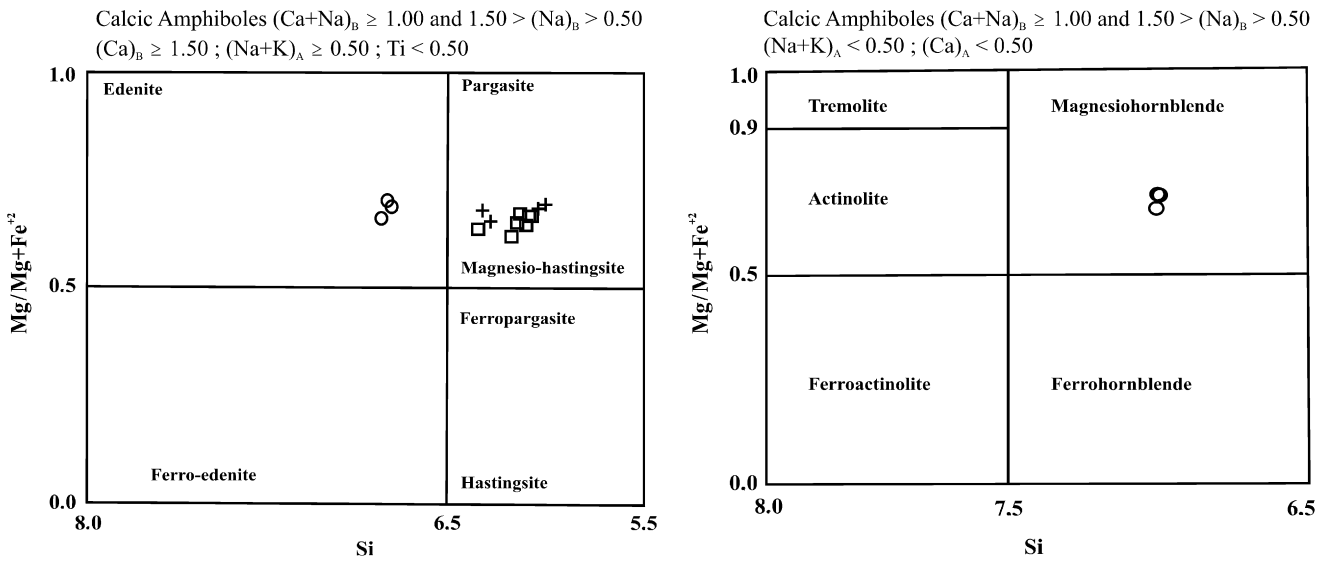

Fig. 5. Nomenclature of calcic amphiboles according to Leake et al. (1997). Square: hornblende andesite, circle: dacite, plus: dacite porphryr.

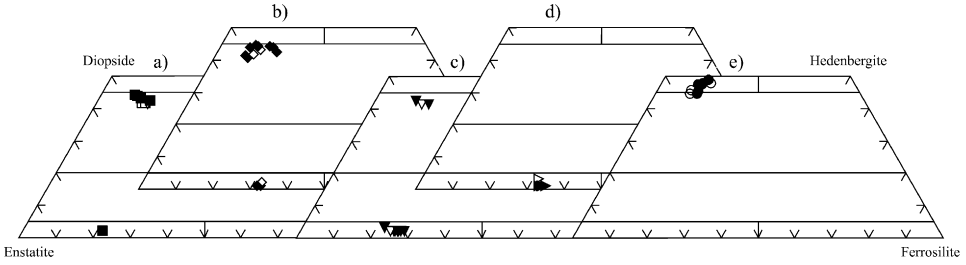

Fig. 6. Nomenclature of pyroxenes according to Morimoto et al. (1988). Solid symbol: core, open symbol: rim. (a) Hornblende andesite, (b) Pyroxene andesite, (c) Trachyandesite, (d) Dacite, (e) Alkali basalt.

behavior can be related to magma mixing (Sakuyama, 1979). Quartz xenocrysts surrounded by radiating needles of pyroxene are at time observed in these rocks. Fe–Ti oxides are ulvöspinels (Fig. 7).

Dacites display vitrophyric porphyritic texture with phenocrysts of plagioclase, amphibole, orthopyroxene, quartz and subordinate Fe–Ti oxide. The groundmass has a hyaline, in places spherulitic texture. Plagioclase is andesine (An_{37-49}) (Fig. 4), with normal and oscillatory zoning. Amphibole is zoned with cores of edenite (Mg# = 0.68) and rims of magnesio-hornblende (Mg# = 0.71), (Fig. 5). Orthopyroxene is enstatite (Fig. 6), with $Wo_{2-4}En_{64-66}Fs_{32-34}$ and Mg# = 0.66–0.68. Fe–Ti oxides conform to the magnetite-ulvöspinels (Fig. 7).

Dacite porphyries display a holocrystalline texture with phenocrysts of plagioclase, amphibole and minor Fe–Ti oxide. The groundmass has a microgranular texture and includes plagioclase, quartz and Fe–Ti oxide. Plagioclase is andesine to labradorite (An_{36-56}) (Fig. 4), with normal and oscillatory zoning. In plagioclase, sieve texture, overgrowths and resorption are widespread. Amphibole is Ti-pargasite (Fig. 5), showing high degree of opacitization. Fe–Ti oxides are magnetite-ulvöspinels (Fig. 7).

5.2. Alkaline volcanites

Alkaline volcanites of the Karacadağ area consist of alkali basalts, of trachybasalts which have higher K_2O contents than alkali basalt in their bulk rock composition (Table 6), and of trachyandesites. Alkali basalt and trachybasalt have similar textures, which vary from holocrystalline to hypocrystalline porphyritic, and the same mineral content with phenocrysts of olivine, clinopyroxene and plagioclase. The groundmass has an intergranular texture and contains plagioclase, clinopyroxene, olivine and Fe–Ti oxide. The olivines with core compositions of Fo_{81-89} and rim composition of Fo_{77-84} display widespread alteration to iddingsite. Clinopyroxene is diopside (Fig. 6), having core

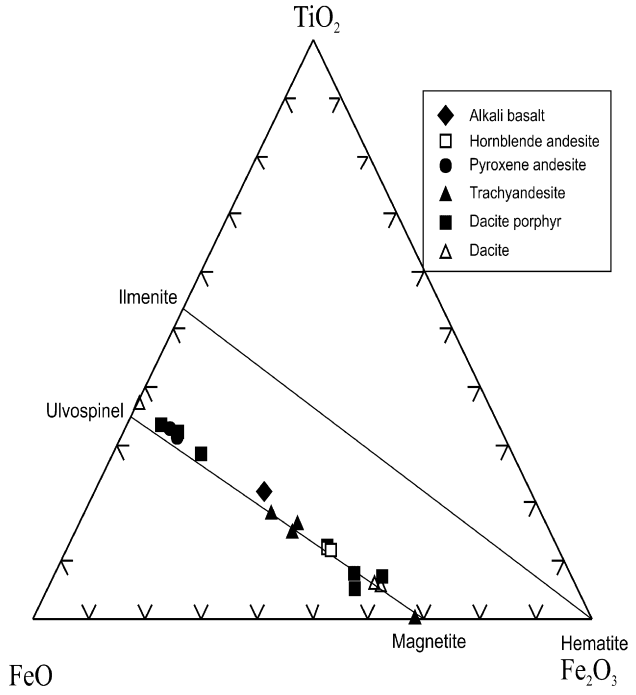

Fig. 7. Fe–Ti oxide composition plot (Bacon and Hirschmann, 1988) of investigated volcanic rocks.

compositions of $Wo_{45-48}En_{41-44}Fs_{10-13}$ and rim compositions of $Wo_{45-48}En_{39-46}Fs_{9-14}$. Plagioclase is labradorite to bytownite (An_{63-71}) (Fig. 4). Fe–Ti oxides are spinel-ulvospinel in composition (Fig. 7).

Trachyandesites have textures which change from hypocrystalline to vitrophyric porphyritic with plagioclase, ortho and clinopyroxene phenocrysts. The groundmass has generally a trachytic, texture with in places a hyaline one. Plagioclase is labradorite to bytownite (An_{58-74}) (Fig. 4), with normal and oscillatory zoning. Clinopyroxene shows a slight normal zoning with core compositions of $Wo_{42}En_{46}Fs_{11}$ (Mg# = 0.81) and rim compositions of $Wo_{41}En_{45}Fs_{14}$ (Mg# = 0.78), (Fig. 6). The core composition of the enstatites is $Wo_3En_{73-75}Fs_{22-25}$ (Mg# = 0.78–0.75) whilst the rim composition is $Wo_{2-3}En_{72-73}Fs_{24-25}$ (Mg# = 0.76–0.75). Some orthopyroxene phenocrysts in trachyandesite were mantled by clinopyroxene. Fe–Ti oxides are magnetite in composition (Fig. 7).

6. Geochemistry

Sixty nine samples of volcanic rocks showing little or no alteration have been choosen for whole rock analyses.

Volcanic rocks from the Karacadağ area display a large compositional spread with SiO_2 contents ranging from 48 to 72 wt%. In the total alkali-silica diagram (TAS) after Le Bas et al. (1986), the calcalkaline volcanites mainly plot in the andesite-dacite field while the alkaline volcanites generally fall in the basalt, trachybasalt, basaltic trachyandesite (scoria samples) and trachyandesite fields (Fig. 8).

In the AFM triangle, andesitic and dacitic samples fall in the calcalkaline field of Irvine and Baragar (1971) and conform to a typical calcalkaline trend (Fig. 9). The calcalkaline andesitic and dacitic rocks are medium-K in composition (Fig. 10) (Le Maitre, 2002).

6.1. Calcalkaline volcanites

In the Harker variation diagrams, MgO, CaO, FeO^{tot}, TiO_2, P_2O_5, Co, Ni and V are negatively correlated with SiO_2 suggesting fractionation of hornblende, Fe–Ti oxide and apatite (Fig. 11). The Na_2O and K_2O are poorly correlated with SiO_2. So these major oxides are not shown in the diagrams.

In calcalkaline suites, Lambert and Holland (1974) used a CaO versus Y diagram to define J and L type trends, which lead to depletion and enrichment in Y relative to a calcalkaline series standard, respectively. The J and L trends have been termed hornblende (±garnet) and pyroxene controlled differantiation trends, respectively, as these minerals can be critical in determining the trend direction. In the Y versus CaO plot (Fig. 12), nearly all the rocks investigated plot on the Y depleted side of the standard calcalkaline trend, defining a J type trend. This trend suggests that hornblende played an important role in the evolution of the calcalkaline volcanites.

The MORB normalized incompatible trace element patterns of the calcalkaline volcanites show enrichment of the large ionic lithophile elements (LILE) and depletion of high field strength elements (HFSE) (Fig. 13). Negative Nb and Ta anomalies reflect a subduction component in their genesis, and the Ti anomaly may reflect Fe–Ti oxide fractionation during their evolution.

The calcalkaline rocks show highly fractionated spoon-shaped REE patterns with $(La/Lu)_N = 11–21$ for andesitic rocks and $(La/Lu)_N = 7–24$ for dacitic rocks (Fig. 14). Generally, with increasing silica content, depletion in MREE and HREE are increased. This can be explained by fractionation of hornblende. The patterns do not exhibit any significant negative Eu anomaly suggesting that no plagioclase fractionation took place in their evolution.

6.2. Alkaline volcanites

In the Harker variation diagrams, MgO, CaO, FeO^{tot}, TiO_2, Co and Ni are negatively correlated with SiO_2 (Fig. 15). These changes are in accord with fractionation

Table 6. Average major (wt%), trace (ppm) and rare earth (ppm) elements analyses of the Karacadağ volcanites

	Alkali basalt (7)	Trachy basalt (5)	Scoria (4)	Trachy andesite(7)	Pyroxene andesite(12)	Hornblende andesite(14)	Dacite Porphyry(5)	Dacite (10)	Breccia Clast(5)
SiO_2	48.84	50.41	53.82	60.63	60.67	60.59	64.85	64.79	66.24
TiO_2	1.44	1.41	1.27	1.00	0.74	0.79	0.54	0.54	0.52
Al_2O_3	16.07	15.90	17.31	17.15	15.92	16.23	16.44	16.01	16.08
$Fe_2O_3^*$	9.36	8.85	7.78	5.58	5.79	5.76	4.17	4.47	3.55
MnO	0.14	0.14	0.09	0.06	0.08	0.09	0.04	0.06	0.05
MgO	7.24	6.47	3.16	1.51	2.90	2.79	1.01	1.70	1.06
CaO	9.19	8.97	7.77	5.03	6.20	6.14	4.66	4.96	4.50
Na_2O	3.31	3.56	3.79	4.78	3.71	3.82	4.06	3.80	3.82
K_2O	1.38	1.88	1.92	1.87	1.55	1.69	1.44	1.54	1.43
P_2O_5	0.52	0.60	0.53	0.48	0.34	0.40	0.26	0.27	0.21
LOI	2.27	1.60	2.33	1.74	1.93	1.53	2.34	1.74	2.40
Total	99.83	99.87	99.78	99.84	99.84	99.83	99.88	99.88	99.88
Trace elements									
Rb	28.54	43.02	41.15	40.83	39.06	41.80	39.14	36.70	40.00
Cs	2.66	2.78	1.35	1.24	1.46	1.61	0.80	1.80	1.80
Ba	481.84	579.96	764.23	597.89	620.43	755.04	703.24	627.14	584.26
Th	4.59	6.28	8.05	6.19	7.25	8.46	8.54	8.35	7.80
U	1.10	1.42	1.88	1.76	2.08	2.39	2.38	2.56	1.96
Nb	18.96	21.78	19.73	18.47	12.21	13.57	10.94	10.01	11.04
Ta	1.16	1.32	1.18	1.20	0.73	0.84	0.72	0.69	0.68
Sr	760.54	873.64	927.68	590.41	667.78	697.59	615.98	564.09	514.86
Zr	143.47	152.90	159.28	160.69	121.18	136.25	121.06	119.31	133.12
Hf	3.53	3.88	3.68	4.14	3.33	3.63	3.10	3.45	3.64
Y	24.81	24.24	37.63	20.13	16.52	18.65	15.32	15.03	15.22
Sc	24.71	23.20	20.00	9.57	11.92	12.00	8.40	8.50	7.20
V	182.57	180.00	179.50	103.71	110.83	111.86	75.80	80.40	64.00
Cr	229.70	265.48	104.34	9.77	88.38	37.63	12.32	28.05	16.42
Ni	104.06	110.48	28.63	6.86	36.82	16.49	11.88	11.21	8.00
Co	37.60	34.30	20.40	11.99	17.61	15.37	8.28	10.43	7.60
Ga	16.76	16.98	18.85	17.73	17.00	18.04	17.28	17.33	17.28
Rare earth elements									
La	29.34	36.82	59.63	32.23	31.95	35.10	35.52	30.01	29.14
Ce	56.41	68.00	96.03	58.64	59.33	63.19	55.34	53.65	51.76
Pr	6.65	7.90	13.05	6.53	6.42	6.91	5.96	5.68	5.63
Nd	27.26	31.34	49.70	24.70	24.22	26.34	22.78	20.79	20.90
Sm	5.10	5.62	9.38	4.51	4.41	4.51	3.36	3.57	3.62
Eu	1.60	1.68	2.47	1.27	1.21	1.22	1.02	0.98	0.99
Gd	5.03	5.24	7.90	3.79	3.45	3.88	3.34	2.88	3.07
Tb	0.73	0.72	1.08	0.58	0.51	0.56	0.45	0.44	0.46
Dy	4.39	4.22	6.45	3.34	2.91	3.23	2.53	2.51	2.74
Ho	0.89	0.90	1.23	0.72	0.51	0.60	0.49	0.46	0.49
Er	2.41	2.37	3.27	1.88	1.51	1.74	1.35	1.40	1.43
Tm	0.37	0.36	0.49	0.29	0.23	0.27	0.22	0.20	0.22
Yb	2.32	2.19	3.15	1.78	1.55	1.70	1.42	1.44	1.52
Lu	0.33	0.31	0.43	0.29	0.22	0.26	0.21	0.21	0.22
Ba/La	16	15	12	18	19	21	19	20	20
Ba/Nb	25	26	38	32	50	55	64	62	52

Fe_2O_3* is the total iron as Fe_2O_3. The numerals in the parentheses show number of analysed sample.

of olivine, clinopyroxene and Fe–Ti oxide. The incompatible major oxides such as Na_2O and K_2O are positively correlated with SiO_2 suggesting fractional crystallization. All these compositional changes are in accord with the observed mineralogy.

The MORB normalized incompatible element patterns of the alkaline basic volcanites (alkali basalt and trachybasalt) display enrichment of elements from Sr to Sm (Fig. 16). However, the spidergram shows marked enrichment of K, Rb, Ba and Th, and a mild enrichment

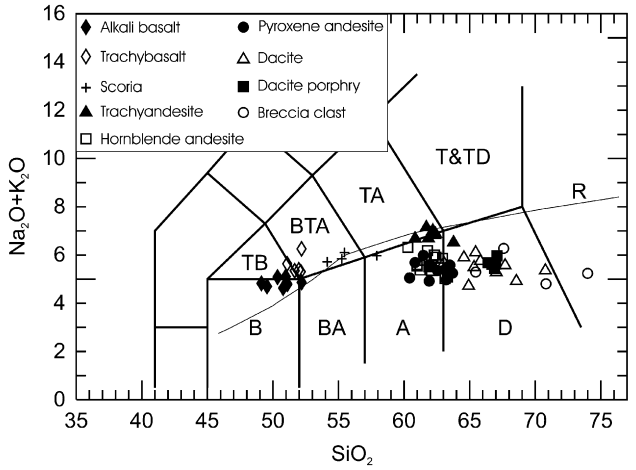

Fig. 8. Total alkali versus silica (TAS) diagram of Karacadağ volcanites (after Le Bas et al., 1986). Solid curved line separates alkaline and subalkaline compositions according to Kuno (1966). B: Basalt, TB: Trachybasalt, BA: Basaltic andesite, BTA: Basaltic trachyandesite, A: Andesite, TA: Trachyandesite, T: Trachyte, TD: Trachydacite, D: Dacite, R: Rhyolite.

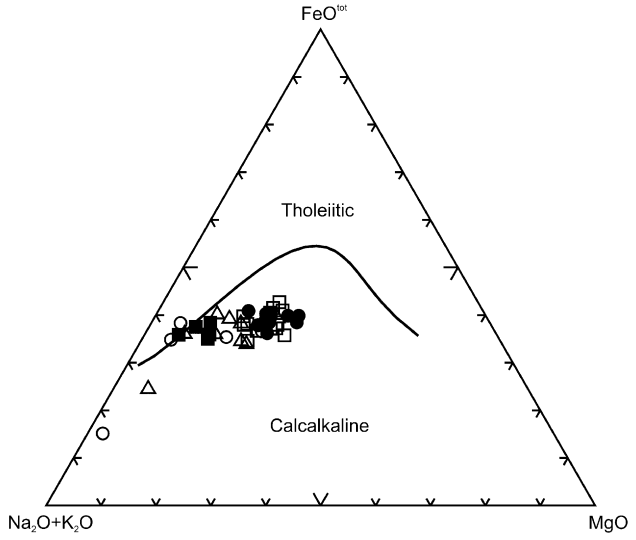

Fig. 9. AFM plot of the studied andesitic-dacitic volcanic rocks (after Irvine and Baragar, 1971). Symbols are as in Fig. 8.

of Sr, Ta, Nb, Ce and P. Scoria and trachyandesite have similar incompatible element patterns suggesting cogenetic relation. The relatively strong incompatible element enrichments in the alkaline volcanites could be due to factors such as an enriched mantle source, small degree of partial melting, degree of fractional crystallization or crustal contamination.

In general, the alkaline rocks show fractionated, slightly concave-upwards REE patterns with $(La/Lu)_N =$

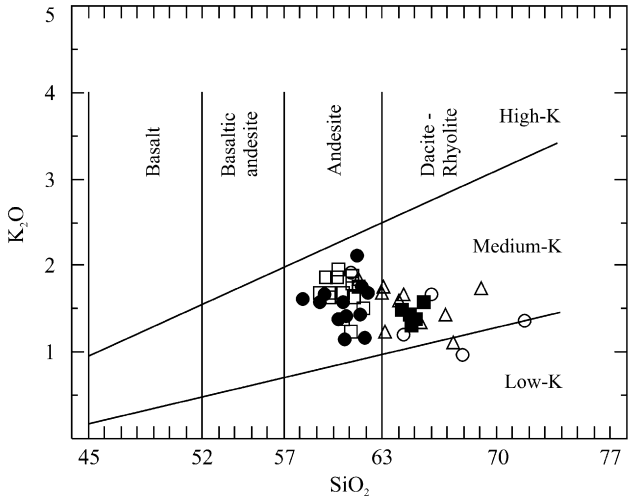

Fig. 10. SiO_2 versus K_2O plot for calcalkaline volcanites of andesitic and dacitic composition (after Le Maitre, 2002). Symbols are as in Fig. 8.

6–17, which is less fractionated than the calcalkaline volcanites (Fig. 17). Also, the rocks have hardly horizontal HREE patterns with $(Ho/Lu)_N =$ 0.9–1.6. The flat HREE patterns of alkali basalts are not consistent with presence of garnet or amphibole in the source (Hanson, 1980). There is no negative Eu anomaly, suggesting that plagioclase fractionation was not important in the evolution of the alkaline volcanites.

To identify dominant magmatic processes controlling the evolution of the volcanites, the process identification diagrams developed by Minster and Allegre (1978) and Allegre and Minster (1978) can be used. In the K/Y vs. K, Ba/Zr vs. Ba and Ba/Y vs. Ba diagrams (Fig. 18), all alkaline volcanites lie along linear trends that pass nearly through the origin. This suggest that fractionation was the main magmatic process in the alkaline volcanites.

A partial melting diagram can be used to better understand the intraplate process and to define the composition of a possible reservoir. On the Zr/Y vs. Zr/Nb diagram (Fig. 19), small degrees of melting have high Zr/Y and low Zr/Nb for the melts whereas large degrees of melting have high Zr/Nb and low Zr/Y magmas (Menzies and Kyle, 1990). In Fig. 19, the variation in Zr/Y versus Zr/Nb is plotted for basaltic volcanic rocks including alkali basalt and trachybasalt and variation is compared with plume-, transitional- and normal-type MORB (Le Roex, 1987). The basaltic samples from the alkaline volcanites indicate small degrees of partial melting of an enriched mantle source.

6.3. Geotectonic settings of the volcanites

In order to determine the geotectonic setting of the calcalkaline volcanites, the La/10-Nb/8-Y/15 digram of

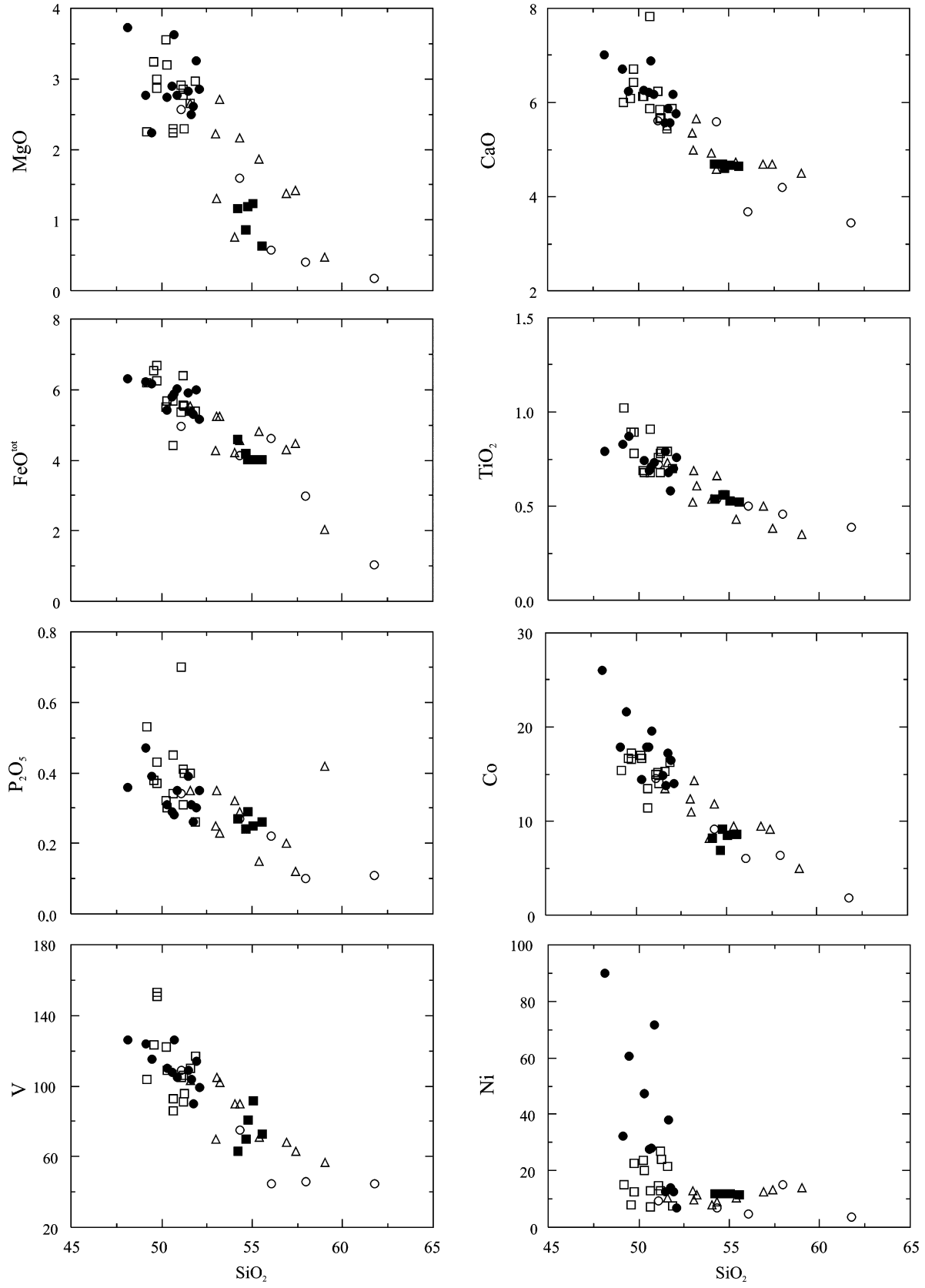

Fig. 11. SiO_2 versus major oxide (%) and trace (ppm) element variation plots of the calcalkaline volcanites. Symbols are as in Fig. 8.

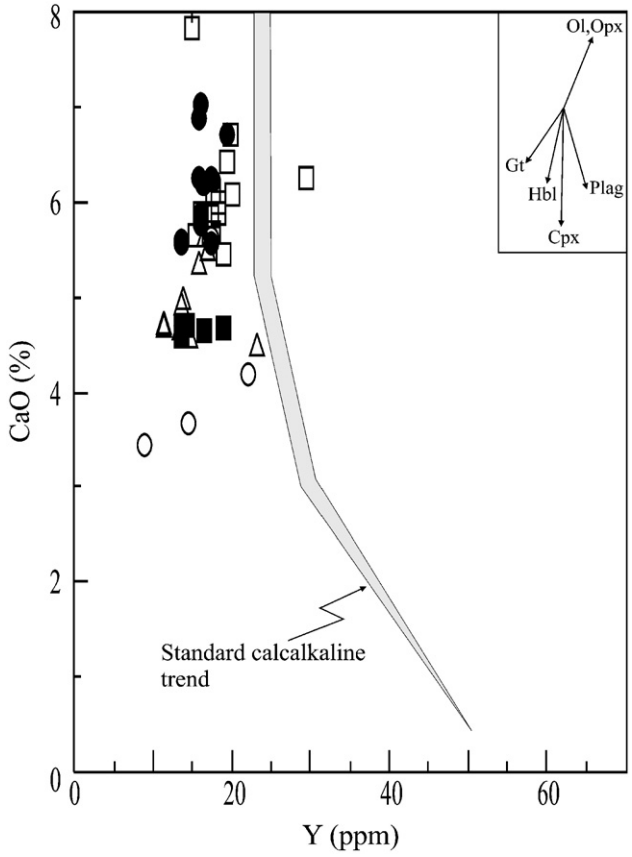

Fig. 12. Y versus CaO plot for the calcalkaline volcanites. Shaded area represents the "standard" calcalkaline trend of Lambert and Holland (1974). The vectors show qualitative trends of the effect of fractional crystallization of common silicates. Symbols are as in Fig. 8.

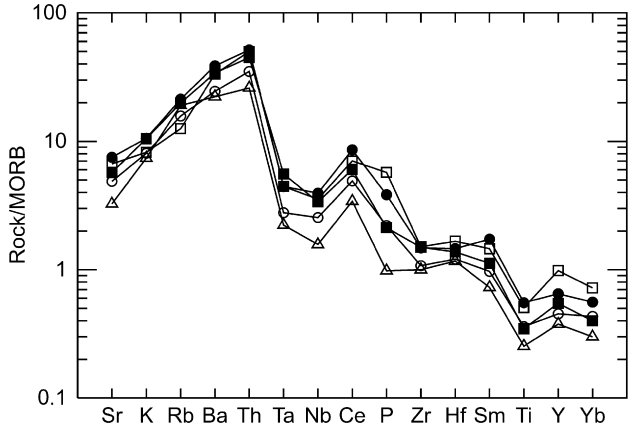

Fig. 13. MORB (Pearce, 1983) normalized trace element patterns of the representative calcalkaline volcanic samples. Symbols are as in Fig. 8.

Cabanis and Lecolle (1989) was used (Fig. 20). The samples mostly cluster in the calcalkaline orogenic domain. However, some of the samples fall in the late to post orogenic domain with continental crust influences. Geochemical characteristics of the calcalkaline volcanites are typical of convergent plate margin and/or collision zone volcanites with low TiO_2 and Nb, high LILE and LREE, high Ba/La (>15) and Ba/Nb (>25) (Gill, 1981; Ewart, 1982; Pearce, 1983). Ba/La and Ba/Nb ratios of the rocks range from 15 to 51 and from 30 to 154, respectively.

Basaltic samples (alkali basalt and trachybasalt) of the alkaline suite clearly fall in the Within Plate Basalt field in the Zr/Y–Zr diagram of Pearce and Norry (1979) (Fig. 21). Generally, these rocks have low Ba/La (11–15, a few up to 19) and Ba/Nb (17–25, a few up to 32) ratios. Therefore, basaltic samples are thought to have no relations with the subduction zone volcanic rocks.

6.4. Isotope geochemistry

The calcalkaline samples display $^{87}Sr/^{86}Sr(t)$ ratios for $t = 18$ Ma between 0.704448 and 0.704889, and $\varepsilon_{Nd}(t)$ values between +2.25 and +3.81, alkaline samples have $^{87}Sr/^{86}Sr(t)$ ratios of 0.703782 to 0.705129 and $\varepsilon_{Nd}(t)$ values between +4.49 and +2.52. In the Sr–Nd diagram, the isotopic data of Karacadağ volcanites are placed on the mantle array between prevelant mantle (PREMA) and bulk silicate earth (BSE) (Fig. 22). Also, some volcanites from Central Anatolia are plotted in the diagram for comparison. The Karacadağ volcanites fall in the field of the Early Miocene Galatian volcanites.

7. Summary and conclusions

^{39}Ar–^{40}Ar dating of the Karacadağ volcanites indicate that volcanism in the Karacadağ area occurred during Early Miocene (ca.19–18 Ma). During this short span time, two volcanic suites formed, with calcalkaline and alkaline characters and there was a progressive change from calcalkaline to alkaline volcanism. The calcalkaline volcanic activity is widespread and dominated by andesitic-dacitic lavas associated with pyroclastics. However, alkaline volcanic rocks, including basalt, trachybasalt and trachyandesite, cover a small area. According to field observations, the rocks of calcalkaline suite are capped by lava flows of alkaline rocks. Also, a few alkali basalt dykes crosscut the rocks of calcalkaline suite. Conforming to these field relations, the trachyandesite yielded a distinctly younger ^{39}Ar–^{40}Ar plateau age of 18.1±0.1 Ma than the dacite (19.2±0.1 Ma) and the andesite (19.0±0.1 Ma), whereas the alkali basalt has virtually the same radiometric age (18.8±0.2 Ma) as the calcalkaline volcanites, within the limits of error. This means that the transition from the calcalkaline to the alkaline volcanic activity took place within a very short time span.

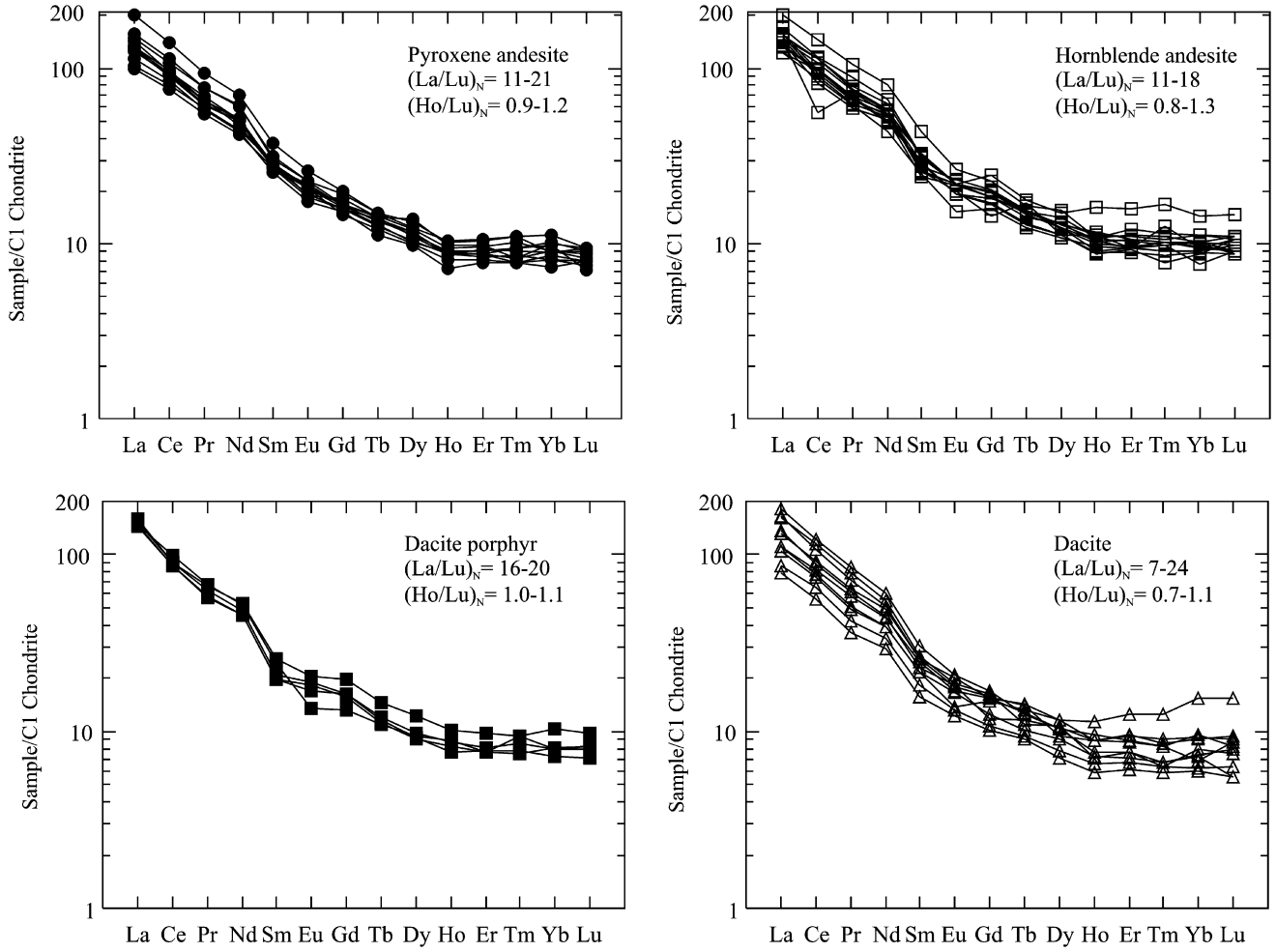

Fig. 14. Chondrite (Sun and McDonough, 1989) normalized rare earth element patterns of the calcalkaline volcanites.

The calcalkaline volcanites are medium-K in character. Chemical variations in the suite suggest that the rocks developed by fractional crystallization of a parent magma. Variations in major and trace element contents are viewed as resulting from fractionation of hornblende, magnetite and apatite. The calcalkaline volcanites show LILE (Sr, K, Rb, Ba and Th) enrichment and relative HFSE depletion with negative Nb, Ta anomalies. They have fractionated spoon shaped REE patterns reflecting hornblende fractionation. The calcalkaline volcanites have relatively low $^{87}Sr/^{86}Sr(t)$ between 0.704448 and 0.704889 isotopic ratios suggesting that crustal contamination did not play an important role in their petrogenesis. Above-mentioned geochemical characteristics of the calcalkaline rocks resemble those for convergent margin lavas related to subduction processes (Gill, 1981; Ewart, 1982; Pearce, 1983). However, in Central Anatolia an active subduction is so far not known in Miocene times. Therefore, the origin of the calcalkaline volcanites could be explained by partial melting of a mantle source modified by previous subduction.

In the alkaline suite, geochemical variations can be explained by fractional crystallization of the observed phenocryst phases, olivine, clinopyroxene and Fe–Ti oxide. MORB normalized trace element patterns are characterized by enrichment in all elements. Also, they do not show negative Nb and Ta anomalies suggesting that this suite is not related to a subduction process. The suite has moderately fractionated REE patterns. There is no significant Eu anomaly. The process identification diagrams suggest that fractionation was the main magmatic process during their evolution. According to geochemical data, the basaltic rocks of the suite can be interpreted as small degree partial melts of an enriched mantle source. Low $^{87}Sr/^{86}Sr$ isotopic ratios do not support crustal contamination in the evolution of the magma.

The northern branch of the Neo Tethys consisted of the İzmir-Ankara-Erzincan and Inner Tauiride Oceans, which started to close by northward subduction at the beginning of the Late Cretaceous (Şengör and Yılmaz, 1981). Through this subduction process, the lithospheric mantle was metasomatically enriched. Presumably, the

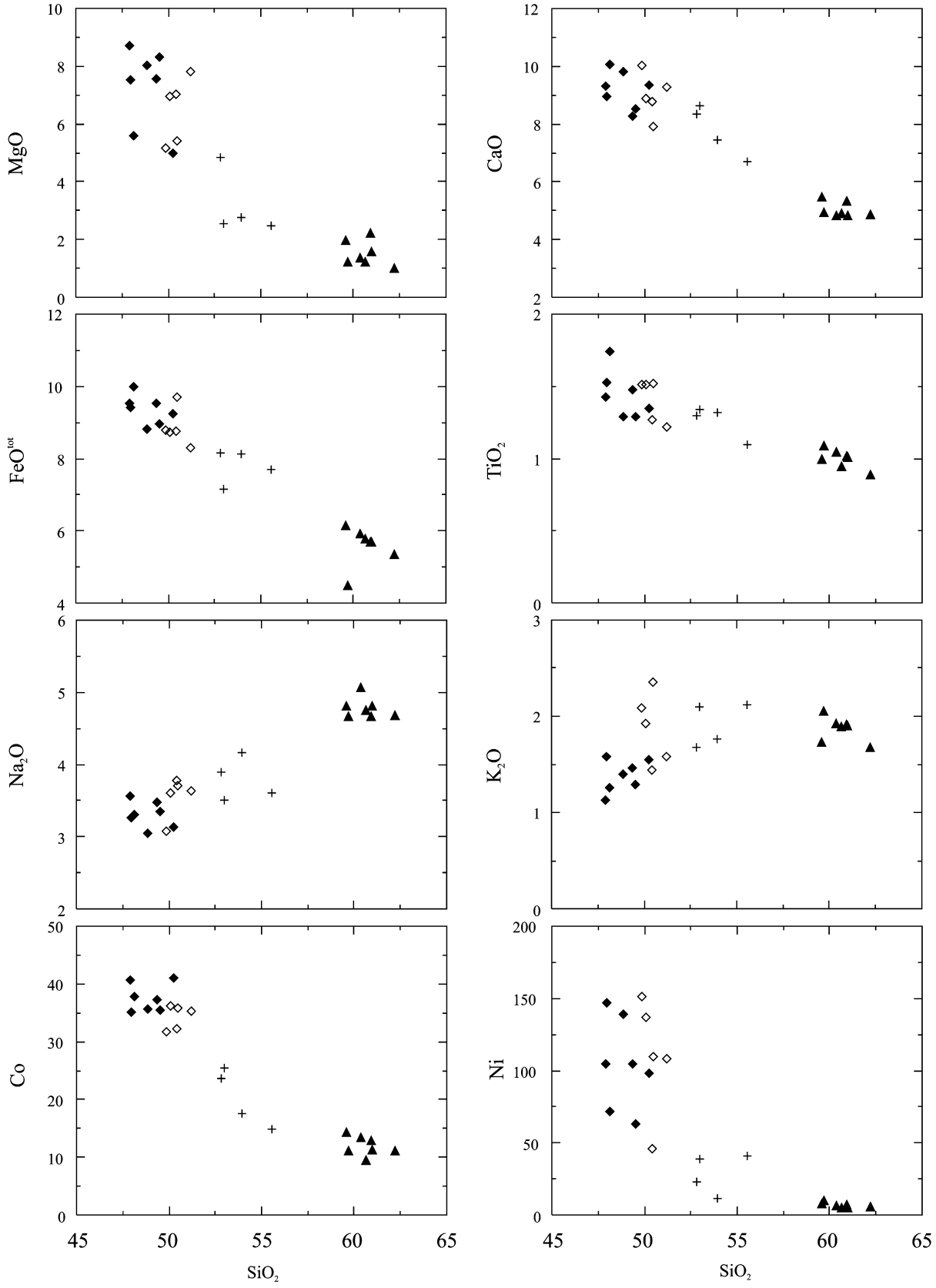

Fig. 15. SiO_2 versus major oxide (%) and trace (ppm) element variation plots of the alkaline volcanites. Symbols are as in Fig. 8.

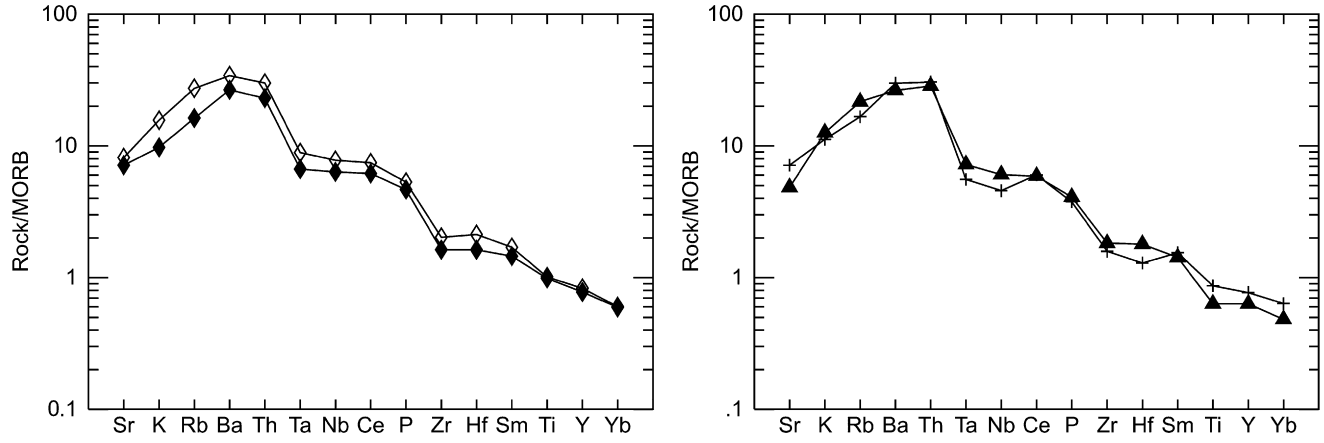

Fig. 16. MORB (Pearce, 1983) normalized trace element patterns of the representative alkaline volcanic rock samples. Symbols are as in Fig. 8.

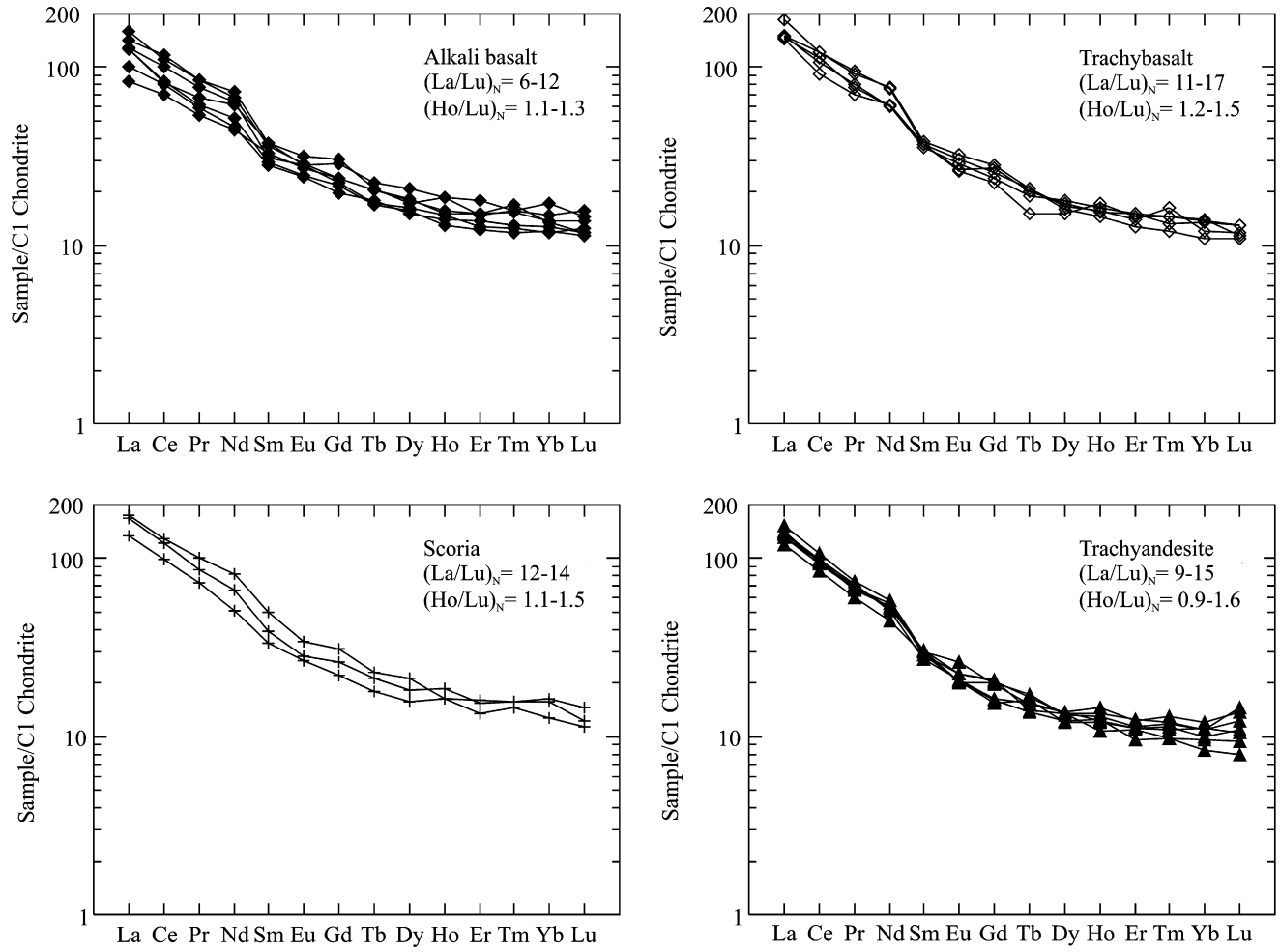

Fig. 17. Chondrite (Sun and McDonough, 1989) normalized rare earth element patterns of the alkaline volcanites.

arc type geochemical signature of the intermediate to acidic calkalkaline Karacadağ volcanites was the heritage of this early subduction of the Neo Tethys. However, the basic to intermediate alkaline Karacadağ volcanites clearly show within-plate signature instead of subduction. Therefore, geochemical characteristics of alkali basalts require a lithospheric source enriched by small volumes of melt from the astenosphere. Many

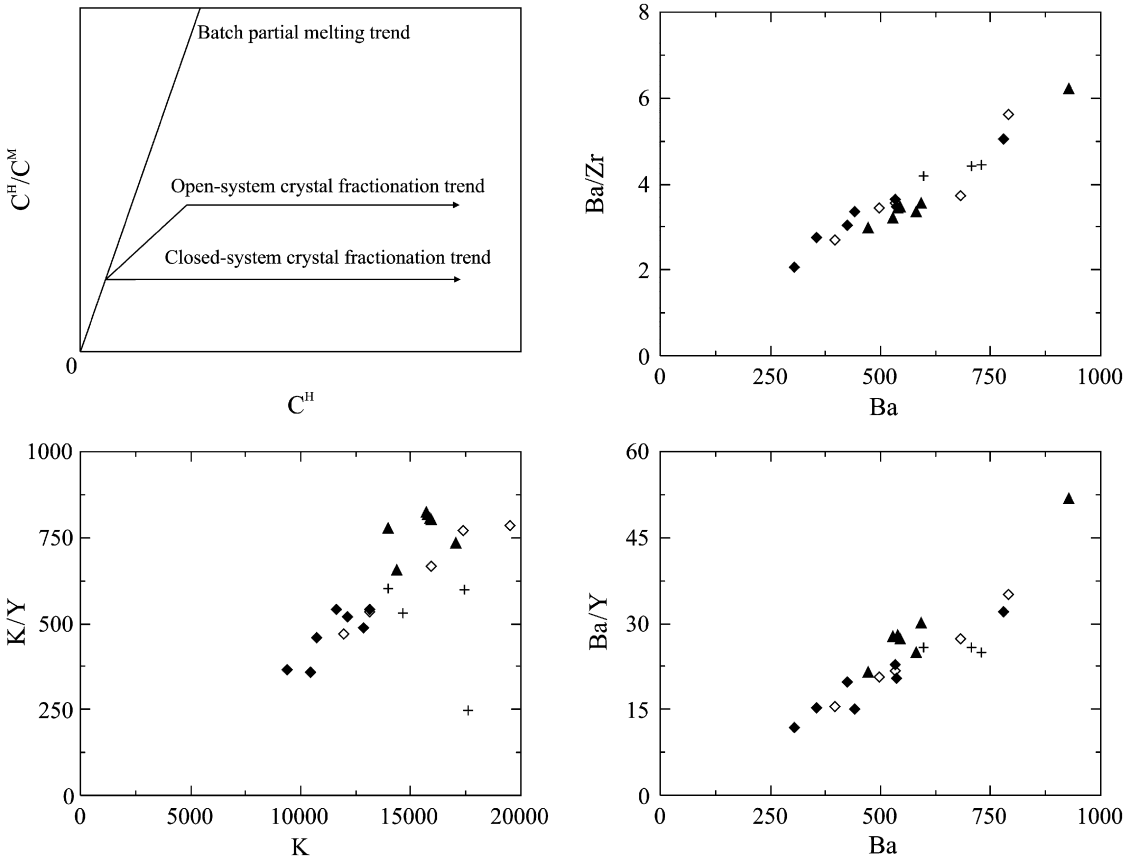

Fig. 18. Process idendification plots based on the relative concentration of moderately (C^M) and highly incompatible (C^H) elements. Symbols are as in Fig. 8.

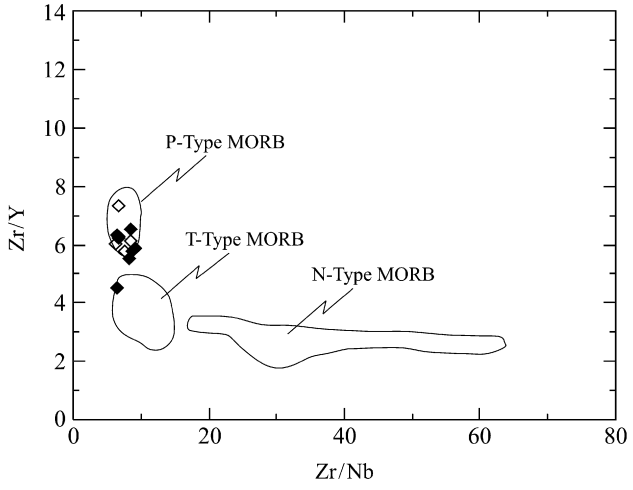

Fig. 19. Zr/Y versus Zr/Nb plot as a measure of amount of partial melting involved in the genesis of the alkaline volcanites. The fields of N-, T-, P- type MORBs are taken from Le Roex (1987). Symbols are as in Fig. 8.

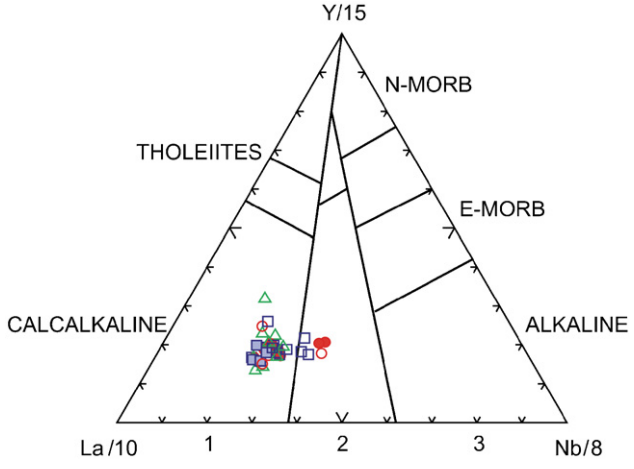

Fig. 20. Y/15-La/10-Nb/8 triangular plot for the calcalkaline volcanites. Fields are 1—orogenic domain, 2—late to post-orogenic domain with continental crust influences, 3—non orogenic domain (after Cabanis and Lecolle, 1989). Symbols are as in Fig. 8.

similarities exist between the Karacadağ volcanites and the Galatean volcanites in respect to their age and their geochemical characteristic. Magmatism of the Galatean province is postcollisional, involving progressive lithospheric thinning (Wilson et al., 1997). So, all characteristics of the Karacadağ volcanites suggest a postcollisional volcanism dominated by lithospheric extension.

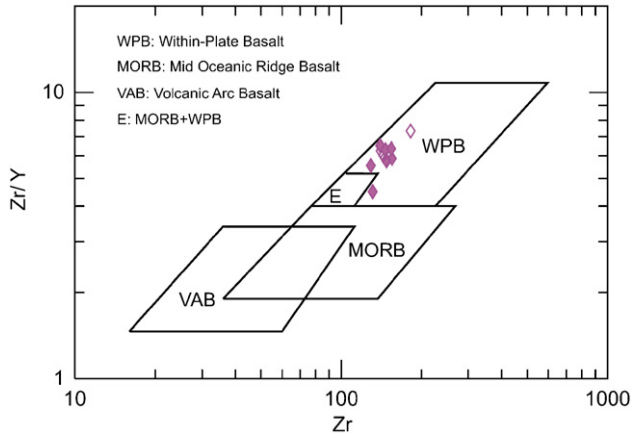

Fig. 21. Zr/Y–Zr tectonic environment discrimination diagram of the alkaline basaltic rocks (after Pearce and Norry, 1979). Symbols are as in Fig. 8.

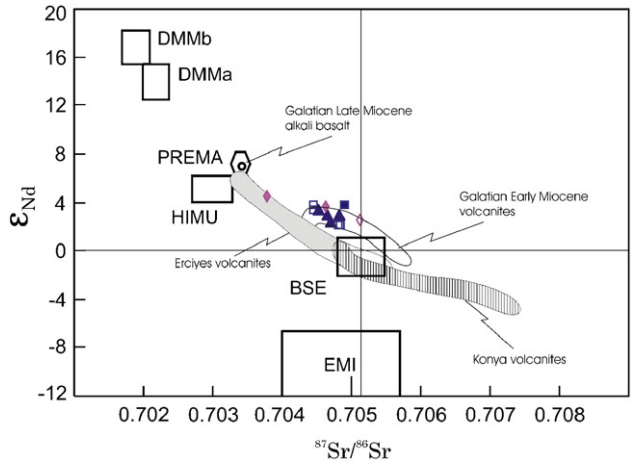

Fig. 22. ε_{Nd} versus $^{87}Sr/^{86}Sr$ diagram for Karacadağ volcanites. DMM: depleted MORB mantle, PREMA: prevelant mantle, HIMU: High μ: mantle, BSE: bulk silicate Earth, EM: enriched mantle. Galatia volcanites from Wilson et al. (1997), Erciyes volcanites from Kürkçüoğlu et al. (1998), Konya volcanites from Temel et al. (1998). Symbols are as in Fig. 8.

Acknowledgements

This study was financially supported by a project numbers 05401043 and 2003/186 from the Selçuk University Coordination of Scientific Research Project (S.Ü. BAP) in Türkiye. The authors gratefully thank to the Selçuk University for its supports. Also, the authors thank to Lang Shi for microprobe analyses (McGill University, Canada), Dean Toye, Clarence Leong and Jacky Wang for ICP-MS and ICP-ES analyses (Acme Laboratories, Canada) and Jean-Jacques Peucat for Sr–Nd isotope analyses (CNRS-Université de Rennes, France). Finally, the authors thank to Professor Dr. Martin Okrusch (Würzburg University) for reviewing the manuscript.

References

Allegre, C.J., Minster, J.F., 1978. Quantitative models of trace element behaviour in magmatic processes. Earth Planet. Sci. Lett. 38, 1–25.

Asan, K., 2002. Karacadağ (Kulu-Konya) yöresi volkanik kayaçlarının petrografik ve jeokimyasal incelemesi. M.Sc. Thesis, Selçuk University, Türkiye, 111pp.

Aydar, E., Gourgaud, A., 1998. The geology of Mount Hasan stratovolcano, central Anatolia, Türkiye. J. Volcanol. Geotherm. Res. 85, 129–152.

Aydar, E., Gourgaud, A., Deniel, C., Lyberis, N., Gündoğdu, M.N., 1995. Le volcanisme quaternaire d'Anatolie central (Turquie): association de magmatisme calco-alcalin et alcalin en domaine de convergence. Canad. J. Earth Sci. 32, 1058–1069.

Bacon, C.R., Hirschmann, M.M., 1988. Mg/Mn partitioning as a test for equilibrium between coexisting Fe–Ti oxides. Am. Mineral. 73, 57–61.

Benito, R., Lopez-Ruiz, J., Cebria, J.M., Hertogen, J., Doblas, M., Oyarzun, R., Demaiffe, D., 1999. Sr and O isotope constraints on source and crustal contamination in the High-K calc-alkaline and shoshonitic Neogene volcanic rocks of SE Spain. Lithos 46, 733–802.

Cabanis, B., Lecolle, M., 1989. Le diagramme La/10, Y/15, Nb/8: un outil pour la discrimination des séries volcaniques et la mise en evidence des processus de mélange et/ou de contamination crustale. C.R. Acad. Sci. Paris 309, 2023–2029.

Dewey, J.F., Hempton, M.R.S., Kidd, W.S.F., Şaroğlu, F., Şengör, A.M.C., 1986. Shortening of continental litosphere: The neotectonics of Eastern Anatolia, a young collision zone. In: Coward, M.P., Ries, A.C. (Eds.), Collison Tectonics, Geological. Society Special Publication vol. 19, pp. 3–36.

Droop, G.T.R., 1987. A general equation for estimating Fe^{3+} concentrations in ferromagnesian silicates and oxides from microprobe analyses using stoichiometric criteria. Mineral. Mag. 51, 431–435.

Duggen, S., Hoernle, K., Van Den Bogaard, P., Garbe-Schönberg, D., 2005. Post-collisional transition from subduction- to intraplate-type magmatism in the westernmost Mediterranean: evidence for continental-edge delamination of subcontinental lithosphere. J. Petrol. 46, 1155–1201.

Eren, Y., Kurt, H., Rosselet, F., Stampfli, G.M., 2004. Paleozoic deformation and magmatism in the northern area of the Anatolide block (Konya), witness of the Palaeotethys active margin. Eclogae Geol. Helv. 97, 293–306.

Ewart, A., 1982. The mineralogy and petrology of Tertiary-Recent orogenic volcanic rocks: with special reference to the andesitic-basaltic compositional range. In: Thorpe, R.S. (Ed.), Andesite: Orogenic Andesite and Related Rocks. Wiley, New York, pp. 25–95.

Gill, J.B., 1981. Orogenic Andesite and Plate Tectonics. Springer, Berlin, 390pp.

Göncüoğlu, M.C., Toprak, V., Kuşçu, İ., Erler, A., Olgun, E., 1991. Orta Anadolu batı kesiminin jeolojisi. Vol. 1. Güney Kesim, Unpublished TPAO Report No. 2909.

Göncüoğlu, M.C., Dirik, K., Erler, A., Yalınız, K., özgül, L., Çemen, İ., 1996. Tuzgölü havzasının batı kısımının temel jeolojik sorunları. Unpublished TPAO Report No. 3753.

Görür, N., Oktay, F.Y., Seymen, İ., Şengör, A.M.C., 1984. Paleotectonic evolution of the Tuzgölü basin complex, Central Türkiye: sedimentary record of a Neo-Tethyan closure. In: Dixon, J.E., Robertson, A.H.F. (Eds.), The Geological Evolution of the Eastern Mediterranean, vol. 17. Geological Society of London Special Publication, Publication, pp. 467–482.

Granet, M., Wilson, M., Achauer, U., 1995. Imaging a mantle plume beneath the French Massif Central. Earth Planet. Sci. Lett. 136, 281–296.

Hanson, G.N., 1980. Rare earth elements in petrogenetic studies of igneous systems. Ann. Rev. Earth Planet. Sci. 8, 371–406.

Hawkesworth, C.J., Gallagher, K., Hergt, J.M., McDermott, F., 1993. Mantle and slab contributions in arc magmas. Ann. Rev. Earth Sci. 21, 175–204.

Hoernle, K., Zhang, Y.S., Graham, D., 1995. Seismic and geochemical evidence for large-scale mantle upwelling beneath the eastern Atlantic and western central Europe. Nature 374, 34–39.

Innocenti, F., Mazzuoli, R., Pasquare, G., Radicati di Brozolo, F., Villari, L., 1975. The Neogene calc-alkaline volcanics of Central Anatolia: geochronological data on Kayseri-Niğde area. Geol. Mag. 112, 349–360.

Irvine, T.N., Baragar, W.R.A., 1971. A guide to the chemical classification of the common volcanic rocks. Canad. J. Earth Sci. 8, 523–548.

Keller, J., Jung, D., Eckhardt, F.-J., Kreuzer, H., 1992. Radiometric ages and geochemical characterization of Galatean andesite massif, Pontus, Türkiye. Acta Vulcanol. 2, 267–276.

Ketin, İ., 1983. Türkiye genel jeolojisine bir bakış. ITU Press, Istanbul, Türkiye.

Koçyigit, A., 1991. Changing stress orientation in progressive intercontinental deformation as indicated by the Neotectonics of the Ankara region (NW Central Anatolia). Bull. Turkish Ass. Petr. Geol. 31, 48–55.

Kuno, H., 1966. Lateral variation of basalt magma types across continental margins and island arcs. Bull. Volcanol. 29, 195–222.

Kurt, H., özkan, A.M., Koçak, K., 2003. Geology, petrography and geochemistry of the subduction related volcanic rocks, West of Konya, Central Anatolia. Geol. Bull. Türkiye 46, 39–51.

Kürkçüoğlu, B., Şen, E., Aydar, E., Gourgaud, A., Gündoğdu, N., 1998. Geochemical approach to magmatic evolution of Mt. Erciyes stratovolcano Central Anatolia, Türkiye. J. Volcanol. Geotherm. Res. 85, 473–494.

Lambert, R.S.J., Holland, J.G., 1974. Yttrium geochemistry applied to petrogenesis utilizing calcium-yttrium relationships in minerals and rocks. Geochim. Cosmochim. Acta 38, 1393–1414.

Leake, B.E., Woolley, A.R., Arps, C.E.S., Birch, W.D., Gilbert, M.C., Grice, J.D., Hawthorne, F.C., Kato, A., Kisch, H.J., Krivovichev, V.G., Linthout, K., Laird, J., Mandaring, J.A., Maresch, W.V., Nickel, E.H., Rock, N.M.S., Schumacher, J.C., Smith, D.C., Stephenson, N.C.N., Ungaretti, L., Whittaker, E.J.W., Youzhi, G., 1997. Nomenclature of amphiboles: report of subcomittee on amphiboles of the International Mineralogical Association, Comission on New Minerals and Mineral Names. Can. Min. 35, 219–246.

Le Bas, M.J., Le Maitre, R.W., Streckeisen, A., Zanettin, B., 1986. A chemical classification of volcanic rocks based on total alkali-silica diagram. J. Petrol. 27, 745–750.

Le Maitre, R.W. (Ed.), 2002. A classification of igneous rocks and glossary of terms. Recommendations of the International Union of Geological Sciences Subcommission on the Systematics of Igneous Rocks. Cambridge University Press, Cambridge, 236pp.

Le Roex, A.P., 1987. Source regions of mid-ocean ridge basalts; evidence for enrichment processes. In: Menzies, A.M., Hawkesworth, C.J. (Eds.), Mantle Metasomatism. Academic Press, London, pp. 389–422.

McKenzie, D., 1972. Active tectonics of Mediterranean Region. Geophys. J. R. Astron. Soc. 30, 109–185.

Menzies, M., Kyle, P.R., 1990. Continental volcanism: a crust-mantle probe. In: Menzies, A.M. (Ed.), Continental Mantle. Clarendon Press, Oxford, pp. 157–177.

Minster, J.F., Allegre, C.J., 1978. Systematic use of trace elements in igneous processes. Part III: Inverse problem of batch partial melting in volcanic studies. Contrib. Mineral. Petrol. 68, 37–52.

Morimoto, N., Fabries, J., Ferguson, A.K., Ginzburg, I.V., Ross, M., Seifert, F.A., Zussman, J., Aoki, K., Gottardi, G., 1988. Nomenclature of pyroxenes. Am. Mineral. 73, 1123–1133.

Okay, A.I., 1986. High-pressure/low temperature metamorphic rocks of Türkiye. In: Ewans, B.W., Brown, E.H. (Eds.), Blueschists and Eclogites. Geol. Soc. Amer. Mem. 164, 338–348.

Okay, A.I., Satir, M., Maluskı, H., Sıyanko, M., Metzger, R., Akyüz, H.S., 1996. Palaeo- and Neo-Tethyan events in northwest Türkiye: geological and geochronological constraints. In: An, Y., Harrison, M. (Eds.), Tectonics of Asia. Cambridge University Press, Cambridge, UK, pp. 420–441.

Pasquare, G., Poli, S., Vezzoli, L., Zanchi, A., 1988. Continental arc volcanism and tectonic setting in Central Anatolia, Türkiye. Tectonophysics 146, 217–230.

Pearce, J.A., 1983. Role of the sub-continental lithosphere in magma genesis at active continental margins. In: Hawkesworth, C.J., Norry, M.J. (Eds.), Continental Basalts and Mantle Xenoliths. Shiva, Nantwich, pp. 230–249.

Pearce, J.A., Norry, M.J., 1979. Petrogenetic implications of Ti, Zr, Y and Nb variations in volcanic rocks. Contrib. Mineral. Petrol. 69, 33–47.

Pearce, J.A., Peate, D.W., 1995. Tectonic implications of the composition of volcanic arc magmas. Ann. Rev. Earth Sci. 23, 251–285.

Renne, P.R., Swisher, C.C., Deino, A.L., Karner, D.B., Owens, T.L., DePaolo, D.J., 1998. Intercalibration of standards, absolute ages and uncertainties in $^{40}Ar/^{39}Ar$ dating. Chem. Geol. 145, 117–152.

Ruffet, G., Féraud, G., Balèvre, M., Kiénast, J.-R., 1995. Plateau ages and excess argon in phengites: an ^{40}Ar–^{39}Ar laser probe study of Alpine micas (Sesia Zone, Western

Alps, northern Italy). Chem. Geol. (Isotopic Geosci. Section) 121, 327–343.

Ruffet, G., Gruau, G., Ballèvre, M., Féraud, G., Philippot, P., 1997. Rb-Sr and ^{40}Ar–^{39}Ar laser probe dating of high-pressure phengites from the Sesia zone (western Alps): underscoring of excess argon and new age constraints on the high-pressure metamorphism. Chem. Geol. 141, 1–18.

Sakuyama, M., 1979. Evidence of magma mixing: petrological study of Shirovma-oike calcalkaline andesite volcano, Japan. J. Volcanol. Geotherm. Res. 5, 179–208.

Stampfli, G.M., Borel, G.D., 2002. A plate tectonic model for the Paleozoic and Mesozoic constrained by dynamic plate boundaries and restored synthetic oceanic isochrons. Earth Planet. Sci. Letters 196, 17–33.

Stampfli, G.M., Marcoux, J., Baud, A., 1991. Tethyan margins in space and time. In: Channell, J.E.T., Winterer, E.L., Jansa, L.F. (Eds.), Palaeogeography and Palaeoceanography of Tethys, Palaeogeog. Palaeocl. Palaeoec. 87, 373–410.

Stampfli, G.M., Mosar, J., Favre, P., Pillevuit, A., Vannay, J.-C., 2001. Permo-Mesozoic evolution of the western Tethyan realm: the Neotethys/East-Mediterranean connection. In: Ziegler, P.A., Cavazza, W., Robertson, A.H.F., Crasquin-Soleau, S. (Eds.), PeriTethys Mem. 6: Peritethyan rift/wrench basins and passive margins, IGCP 369. Mem. Mus. Nat. Hist. Nat. Paris, vol.186, pp. 51–108.

Steiger, R.H., Jäger, E., 1977. Subcommission on geochronology: convention on the use of decay constants in geo- and cosmochronology. Earth Planet. Sci. Lett. 36, 359–362.

Sun, S., McDonough, W.F., 1989. Chemical and isotopic systematic of oceanic basalts: implications for mantle compositions and processes. In: Saunders, A.D., Norry, M.J. (Eds.), Magmatism in the Ocean Basins. Geol. Soc. London Spec. Publ. 42, 313–345.

Şenel, M. (Ed.), 2001. Geology Map of Türkiye with 1:500.000 scale. General Directorate of Mineral Research and Exploration, Ankara.

Şengör, A.M.C., 1985. The Cimmeride orogenic system and the tectonics of Eurasia. Geol. Soc. Am. Spec. Publ. 195, 74pp.

Şengör, A.M.C., Yılmaz, Y., 1981. Tethyan evolution of Türkiye: A plate tectonic approach. Tectonophysics 75, 81–241.

Şengör, A.M.C., Görür, N., Şaroğlu, F., 1985. Strike slip faulting and related basin formation in zones of tectonic escape: Türkiye as a case study. In: Biddle, T.R., Christie-Blick, N.N. (Eds.), Strike-slip Deformation, Basin Formation and Sedimentation. Soc. Econ. Paleont. Mineral. Spec. Publ., vol. 37, Oklahama, pp. 227–264.

Tankut, A., Wilson, M., Yihunie, T., 1998. Geochemistry and tectonic setting of tertiary volcanism in the Güvem area, Anatolia, Türkiye. J. Volcanol. Geotherm. Res. 85, 285–301.

Tankut, A., Akıman, O., Türkmenoğlu, A., Güleç, N., Göker, T., 1991. Tertiary volcanic rocks in northwest central Anatolia. Proceedings of IESCA 1990, vol.2, pp.450–466.

Temel, A., Gündoğdu, M.N., Gourgaud, A., 1998. Petrological and geochemical characteristic of Cenozoic high-K calcalkaline volcanism in Konya, Central Anatolia, Türkiye. J. Volcanol. Geotherm. Res. 85, 327–354.

Turner, S., Arnaud, N., Liu, J., Rogers, N., Hawkesworth, C., Harris, N., Kelley, S., Van Calsteren, P., Deng, W., 1996. Post-collision, shoshonitic volcanism on the Tibetan Plateau: implications for convective thinning of the lithosphere and the source of ocean island basalts. J. Petrol. 37, 45–71.

Turner, S., Platt, J.P., George, R.M.M., Kelley, S.P., Pearson, D.G., Nowell, G.M., 1999. Magmatism associated with orogenic collapse of the Betic-Alboran Domain, SE Spain. J. Petrol. 40, 1011–1036.

Wilson, M., Downes, H., 1991. Tertiary–Quaternary extension-related alkaline magmatism in Western and Central Europe. J. Petrol. 32, 811–849.

Wilson, M., Tankut, A., Güleç, N., 1997. Tertiary volcanism of the Galatia province, North-west Central Anatolia, Türkiye. Lithos 42, 105–121.